Role of Ponded Turbidity Currents in Reservoir Trap Efficiency

By Horacio Toniolo[1], Gary Parker[2] and Vaughan Voller[3]

Abstract: The capacity to store water in a reservoir declines as it traps sediment. A river entering a reservoir forms a prograding delta. Coarse sediment (e.g., sand) deposits in the fluvial topset and avalanching foreset of the delta, and is typically trapped with an efficiency near 100 percent. The trap efficiency of fine sediment (e.g., mud), on the other hand, may be below 100 percent, because some of this sediment may pass out of the reservoir without settling out. Here a model of trap efficiency of mud is developed in terms of the mechanics of a turbidity current that plunges on the foreset. The dam causes a sustained turbidity current to reflect and form a muddy pond bounded upstream by a hydraulic jump. If the interface of this muddy pond rises above any vent or overflow point at the dam, the trap efficiency of mud drops below 100 percent. A model of the coevolution of topset, foreset, and bottomset in a reservoir that captures the dynamics of the internal muddy pond is presented. Numerical implementation, comparison against an experiment, and application to a field-scale case provide the basis for a physical understanding of the processes that determine reservoir trap efficiency.

CE Database subject headings: Reservoirs, Sediment transport, Turbidity currents, Experimentation, Numerical models.

[1] Asst. Prof., Dept. of Civil and Environmental Engineering, University of Alaska, Fairbanks, AK 99775, email: ffhat@uaf.edu

[2] Prof., Depts. of Civil and Environmental Engineering and Geology, University of Illinois, Urbana IL 61801, email: parkerg@uiuc.edu

[3] Prof., Dept. of Civil Engineering, University of Minnesota, Minneapolis MN 55414, email: volle001@umn.edu

Introduction

Sediment deposition in a reservoir reduces its storage capacity (Graf 1971; Fan and Morris 1992). Sediment accumulation has been estimated to decrease worldwide reservoir storage by 1% per year (Mahmood 1987; Sloff 1997). The sediment trap efficiency of an impoundment on a sand-bed river is considered here. Sand-bed rivers typically transport not only sand-sized sediment, but also silt- and clay-sized sediment as well. These two finer sizes, here lumped together as "mud," are typically transported as wash load. When the river enters the backwater zone of an impoundment its sediment deposits to form a delta. The sand mostly deposits fluvially to form a topset, and by avalanching to form a foreset. The mud mostly deposits beyond the toe of the foreset to form a bottomset in deep water, as illustrated in Fig. 1. The reservoir fills as the topset and foreset prograde downstream and the bottomset builds upward. Fig. 2 shows the history of evolution of the delta of the Colorado River at Lake Mead (Smith et al. 1960).

A reservoir on a sand-bed stream typically traps sand in the topset and foreset with near 100 percent efficiency until such time as the foreset reaches the dam itself. Mud, on the other hand, can often be vented from a reservoir long before the foreset reaches the dam. Muddy water can move into the body of the reservoir as one of three flows; a surface plume, an interflow, or a bottom turbidity current that forms by plunging (e.g., Fig. 4.5 of Morris and Fan 1997). The case of plunging is considered here (Fig. 1). When the muddy river water is heavier than the bottom water of the reservoir, it plunges just beyond the topset-foreset break to form a bottom turbidity current. Plunging has been observed by many authors (e.g., Forel 1885; Grover and Howard 1937; Bell 1942; Lane 1954; Normark and Dickson 1976; Lambert 1982; Chikita 1989; Fan and Morris 1992; De Cesare et al. 2001).

The turbidity current created by plunging is supercritical in the sense that the densimetric Froude number $\boldsymbol{Fr}_d$ is greater than unity. Here

$$\boldsymbol{Fr}_d = \frac{U_t}{\sqrt{R_m g C_t H_t}} \tag{1}$$

and H_t = layer thickness of the turbidity current, U_t = layer-averaged velocity of the turbidity current, C_t = layer-averaged volume concentration of suspended mud in the turbidity current and g = acceleration of gravity. In addition R_m = submerged specific gravity of the mud in the turbidity current = $(\rho_{sm}/\rho) - 1$, where ρ = water density and ρ_{sm} = material density of the mud.

In the case of long reservoirs the turbidity current can move several tens of kilometers downstream (Fan and Morris 1992; Twichell et al. 2005). If the current reaches the dam, and is not vented, the head of the current runs up against the face of the dam and forms a backward-migrating bore (e.g., Bell 1942). This bore eventually stabilizes in the form of an internal hydraulic jump, downstream of which an internal muddy pond forms (e.g., Fig. 24 of Bell 1942). The turbidity current within the ponded zone is subcritical, i.e., $\boldsymbol{Fr}_d < 1$. If the pond is sufficiently deep, i.e., if $\boldsymbol{Fr}_d << 1$ within it, a fairly sharp horizontal interface evolves, with muddy water below and ambient water above. The quasi-steady flow associated with the formation of a muddy pond is illustrated in Fig. 1. Both Bell (1942) and Morris and Fan (1997) mention the formation of internal muddy ponds in reservoirs. Here the issue of sediment trap efficiency is addressed in terms of the dynamics of the muddy pond.

One of several standard diagrams for computing trap efficiency is the Brune (1953) diagram. Simply put, the Brune diagram indicates that the longer the residence time of water in the reservoir, the greater is its trap efficiency. The Brune (1953) diagram has, however, an obvious deficiency; the sediment input rate in no way enters into the computation of trap efficiency. In addition, the Brune diagram is an empirical tool which does not incorporate the physics describing how sediment is trapped in reservoirs. The present work provides a partial basis for rectifying these deficiencies.

Role of the Muddy Pond

The role of the muddy pond in reservoir sedimentation came to the attention of the authors from of a seemingly unrelated field, i.e., sedimentation due to turbidity currents flowing into submerged basins on the continental slope of the ocean (Toniolo et al. in press(a), in press(b)). Consider a sustained, turbidity current spilling into a submerged basin, as illustrated in Fig. 3. The inflowing turbidity current is assumed to be supercritical, i.e., $\boldsymbol{Fr}_d > 1$. If the relief of the basin is sufficient, the flow eventually reaches a quasi-equilibrium configuration with a hydraulic jump to a muddy pond containing flow that is subcritical, i.e., $\boldsymbol{Fr}_d < 1$. Toniolo et al. found that two quasi-equilibrium states are possible, both of which are illustrated in Fig. 3. In the first of these the turbidity current overflows the downstream lip of the basin and basin trap efficiency is less than 100 percent. In the second of these, however, the turbidity current cannot escape the basin even though the inflow is sustained, because the interface between the muddy pond and the clear water above equilibrates at a position that is below the elevation of the downstream lip. The basin trap efficiency is then equal to 100 percent.

On face value, the condition for 100 percent trapping in Fig. 3, i.e., a continuous inflowing current but no outflow current would appear to contradict mass conservation. The contradiction is resolved in terms of water detrainment from a muddy layer. Consider a dilute, uniform suspension of mud of uniform size and fall velocity v_{sm} that is allowed to settle out in a cylinder of cross-sectional area A (Fig. 4). Within a short time a settling interface forms. The settling interface moves downward with the fall velocity v_{sm} of the mud. As it does so, water is detrained from the muddy layer to the clear layer above at a detrainment discharge Q_d given as

$$Q_d = v_{sm} A \tag{2}$$

Now consider a highly ponded turbidity current delineated by an internal jump upstream and a barrier downstream, as shown in Fig. 3. Deep ponding, which is characterized by a very low densimetric Froude number $\boldsymbol{Fr}_d$, ensures that turbulence gradually dies out beyond the hydraulic jump. Sediment settles out passively, and water detrains upward across the settling interface. The interface need not change position in time, however, if the detrained water is being constantly replaced by an upstream inflow. If the detrainment discharge across the interface is less than the inflow discharge of water, the interface is located above the lip of the downstream barrier, and both water and sediment overspill in the form of an outflowing turbidity current.

If, however, the potential for detrainment is sufficiently large, water detrainment consumes the entire inflow. The interface is then located below the downstream lip, in which case no outflowing current forms, and all the inflowing sediment is trapped in the basin. Such a quasi-steady flow with complete trapping of the sediment can be sustained until such time as sediment deposition itself raises the interface above the downstream lip.

Toniolo et al. (in press(a), in press(b)) have verified this picture with the aid of theory, numerical modeling, and experimentation, and have shown its relevance to the field.

The extension to reservoir sedimentation is clear. If detrainment dictates that the muddy pond of Fig. 1 lie below any overflow point or vent, the trap efficiency of the reservoir is 100 percent. As the foreset progrades and the bottomset builds up, however, the settling interface must slowly rise in time, eventually to the point at which overflow occurs and the trap efficiency drops below 100 percent.

Theory for a Muddy Pond

Configuration, governing equations and boundary conditions

A reservoir with a simplified configuration is considered, i.e., a rectangular slot with width B_r and length L_r such that $B_r/L_r << 1$. A downstream vertical barrier models a dam. The bottom turbidity current is continuous and carries a dilute suspension of mud of uniform size with fall velocity v_{sm}. The turbidity current is supercritical in the sense of the densimetric Froude number just downstream of the plunge point. The barrier causes the turbidity current to reflect, migrate upstream as a bore and stabilize as an internal hydraulic jump, so creating a muddy pond with a very low densimetric Froude number $\boldsymbol{Fr}_d$ containing a dilute suspension of very slowly moving water and sediment (Fig. 1). The interface between the muddy pond and the clear water above defines a settling interface. This interface may be either below the elevation of the lowest overflow point over or vent in the barrier (as drawn in Fig. 1) or above it. In the former case all the mud is lost to bed deposition and all the inflowing water is lost to detrainment across the settling interface.

For the sake of simplicity, one modification is made to the configuration of Fig. 1 before proceeding. The dam of Fig. 5a impounds the water so that all of it flows through a vent into air on the other side. In Fig. 5b this configuration is replaced by a submerged barrier with nearly standing water on the upstream side and standing water on the downstream side. Fig. 5b shows two possible interface positions, the lower one yielding 100 percent trapping of mud and the higher one allowing mud to escape.

Let t = time, x = a bed-attached streamwise coordinate, y = a coordinate directed upward normal from the bed and assumed quasi-vertical, H_t = the thickness of turbid water in the muddy pond (the subscript t denoting "turbidity"), and (u, v) = the local flow velocities in the (x, y) directions (averaged over any turbulence in the ponded zone).

The flow in the ponded zone is assumed to be very slow, and any turbulence within it is assumed to be too weak to entrain a) water across the settling interface, and b) sediment from the bed. In this case the equations of water mass balance, sediment mass balance, and momentum balance take the respective forms

$$\frac{\partial u}{\partial x}+\frac{\partial v}{\partial y}=0$$

$$\frac{\partial c}{\partial t}+\frac{\partial uc}{\partial x}+\frac{\partial vc}{\partial y}-v_{sm}\frac{\partial c}{\partial y}=0 \qquad \text{(3a, b, c)}$$

$$\frac{\partial u}{\partial t}+\frac{\partial u^2}{\partial x}+\frac{\partial uv}{\partial y}=-R_m g\frac{\partial}{\partial x}\int_y^{H_t} c\,dy+R_m g c S_t+\frac{1}{\rho}\frac{\partial \tau}{\partial y}$$

(e.g., Parker et al. 1986). In the above relations c = volume concentration of sediment, here assumed to be small, τ is shorthand for the τ_{xy} component of shear stress and bed slope S_t is given as

$$S_t = -\frac{\partial \eta_t}{\partial x} \tag{3d}$$

where η_t = reservoir bottom elevation. The above relations employ the slender flow approximations, according to which the horizontal extent of the body of ponded turbid water must be much larger than the depth of the ponded zone.

The bed is assumed to be impermeable, so that

$$u\big|_{y=0} = v\big|_{y=0} = 0 \tag{4}$$

The settling interface is described by a variant of the kinematic boundary condition:

$$\frac{\partial H_t}{\partial t} + u\big|_{y=h}\frac{\partial H_t}{\partial x} = v\big|_{y=h} - v_{sm} \tag{5a}$$

In the simple settling tube of Fig. 4, for example, Eq. (5a) reduces to

$$\frac{\partial H_t}{\partial t} = -v_{sm} \tag{5b}$$

so that in the absence of replenishing turbid flow the interface is advected downward with the fall velocity of the sediment.

Integration within the muddy pond

Eqs. (3a-3c) are now integrated from the bed to the settling interface of the ponded zone of Fig. 1. It is assumed that the internal hydraulic jump at the upstream end of the ponded zone has acted to mix the sediment uniformly in the vertical in the muddy pond downstream. Since the very slow flow velocities in a strongly ponded zone dictate passive settling in the absence of resuspension, as one layer of sediment in the water column settles it is replaced from above by another layer with the same concentration. Thus concentration c can be taken as equal to a constant C_t in y between $y = 0$ and $y = H_t$, i.e.

$$c(x,y,t) = \begin{cases} C_t(x,t) & ,0 < y < H_t \\ 0 & ,y > H_t \end{cases} \tag{6}$$

The above assumptions are justified more specifically in the section "Experiment" below. Integrating Eq. (3a) from 0 to H_t with Eq. (4) and Eq. (5a) it found that

$$\frac{\partial H_t}{\partial t} + \frac{\partial U_t H_t}{\partial x} = -v_{sm} \tag{7}$$

where

$$U_t = \frac{1}{H_t}\int_0^{H_t} u\,dy \tag{8}$$

denotes the layer-averaged streamwise flow velocity in the ponded zone. Note that the term - v_{sm} on the right-hand side of Eq. (7) quantifies the rate of loss of water across the settling interface.

A similar integration of Eq. (3b) with the aid of Eqs. (4), (5a) and (6) yields the following:

$$\frac{\partial C_t H_t}{\partial t} + \frac{\partial U_t C_t H_t}{\partial x} = -v_{sm} C_t \tag{9}$$

The corresponding Exner equation of bed sediment conservation takes the form

$$(1-\lambda_{pm})\frac{\partial \eta_t}{\partial t} = v_{sm} C_t \tag{10}$$

where λ_{pm} is the sediment porosity of bottomset. The integral of Eq. (3c) is

$$\frac{\partial U_t H_t}{\partial t} + \frac{\partial U_t^2 H_t}{\partial x} + U_t v_{sm} = -\frac{1}{2} R_m g \frac{\partial C_t H_t^2}{\partial x} + R_m g C_t H_t S_t - C_{fs} U_t^2 \tag{11}$$

In deriving Eq. (11) it has been assumed that local velocity u can be approximated with its layer-averaged value U_t from $y = 0$ to $y = H_t$ in evaluating the last two terms on the left-hand side. In addition, the shear stress at the bed has been related to the square of the flow velocity by means of the bed resistance coefficient C_{fs}. The muddy pond is assumed to be moving sufficiently slowly to allow the neglect of interfacial friction.

Solution for suspended sediment concentration

Cross-eliminating between Eqs. (7) and (9), the relation governing the concentration C_t in the basin becomes;

$$\frac{\partial C_t}{\partial t} + U_t \frac{\partial C_t}{\partial x} = 0 \tag{12a}$$

That is, any given concentration C_t at the upstream end of the basin (i.e., just beyond the hydraulic jump) is advected at velocity U_t without change down the basin. In the case of steady flow, Eq. (12a) reduces to the condition

$$C_t = const \tag{12b}$$

The above relation is of some significance. If the water and sediment input to the basin is steady, the flow in the ponded zone can be treated as quasi-steady, with a constant sediment concentration throughout its length. The flow is not truly steady, because sediment deposition builds the bed upward in time, but in the case of a dilute turbidity current this process is very slow compared to the setup time for the hydraulic jump and ponding. It is seen from Eqs. (10) and (12b) that for quasi-steady conditions the bed in the ponded zone deposits as a layer of uniform thickness.

Water detrainment and outflow

Whether or not the flow spills out of the basin is determined from Eq. (7). The forward volume flow discharge per unit width = q_w, where

$$q_w = U_t H_t \tag{13}$$

Now let the origin of the x coordinate be located just downstream of the hydraulic jump. For a quasi-steady flow Eq. (7) integrates to

$$q_w = q_{wj} - v_{sm} x \tag{14}$$

where q_{wj} denotes the value of q_w just beyond the hydraulic jump. Let L_p denote the length of the ponded zone from the hydraulic jump to the overflow point. Overflow occurs only if

$$q_{wj} - v_{sm} L_p > 0 \tag{15}$$

Condition (15) merits some elaboration. The discharge Q_j of muddy water entering the muddy pond is given as $Q_j = q_{wj} B_r$. The detrainment discharge is then given

as $Q_d = v_{sm} L_p B_r$. In the event that $Q_d < Q_j$, the interface of the muddy pond must equilibrate at a point that allows outflow of muddy water, thus yielding a trap efficiency of less than 100 percent. The precise value of Q_j, however, is crucially dependent upon the position of the hydraulic jump relative to the dam itself, i.e., the length L_p of the ponded zone.

Let Δh denote reservoir relief from the bed elevation at the base of the dam to the lowest overflow point. Increasing inflow discharge Q_j should push the hydraulic jump farther downstream, so reducing Q_d and pushing the pond in the direction of overflow. Decreasing relief Δh due to gradual bottomset buildup over time can be expected to operate in the same direction; by allowing for less of a pressure barrier in the muddy pond it should act to reduce L_p and push the pond in the direction of overflow. The conditions governing the position of the hydraulic jump relative to the dam are discussed in a subsequent section.

Interface Shape

Eq. (11) reduces with Eqs. (3d) and (7) to:

$$\frac{\partial U_t}{\partial t} + U_t \frac{\partial U_t}{\partial x} = -R_m g C_t \left(\frac{\partial \xi_m}{\partial x} + \frac{1}{2} \frac{H_t}{C_t} \frac{\partial C_t}{\partial x} \right) - C_{fs} \frac{U_t^2}{H_t} = 0 \tag{16}$$

where

$$\xi_m = \eta_t + H_t \tag{17}$$

ξ_m = elevation of the settling interface. If the flow is sufficiently slow the quadratic drag term in Eq. (16) may be neglected. (This assumption may break down right near the overflow point, where the flow re-accelerates.) Further assuming steady flow, Eq. (16) reduces with Eq. (12b) to

$$\frac{d}{dx} \left(\frac{1}{2} U_t^2 + R_m g C_t \xi_m \right) = 0 \tag{18a}$$

or thus

$$\frac{1}{2} U_t^2 + R_m g C_t \xi_m = const \tag{18b}$$

i.e., a Bernoulli equation relating layer-averaged flow velocity in the muddy pond to the elevation of its interface.

Wherever the ponded zone is sufficiently deep (and thus $\boldsymbol{Fr}_d$ is sufficiently small), the first term on the left-hand side of Eq. (18b) is small compared to the second term on the left-hand side, resulting in the condition of an interfacial elevation ξ_m that is constant everywhere in space, i.e.

$$\xi_m = const = \xi_{mp} \tag{18c}$$

For the case of sufficient ponding this condition can be expected to be satisfied everywhere except in the vicinity of an overflow point

The turbidity current overflows the barrier of Fig. 5b in the event that Condition (15) is satisfied. Let U_{ts} denote the flow velocity, H_{ts} denote the flow thickness and ξ_{ms} denote the interface elevation at the point of overflow of the downstream barrier. At the point of overflow the densimetric Froude number must be equal to unity, i.e.

$$\frac{U_{ts}^2}{R_m g C_t H_{ts}} = \frac{q_{ws}^2}{R_m g C_t H_{ts}^3} = 1 \tag{19}$$

where $q_{ws} = U_{ts} H_{ts}$ denotes the overflow discharge per unit width. Let ξ_{mp} = the constant elevation of the interface in the ponded zone of the basin, i.e., well upstream of the overflow point, within which the term $\frac{1}{2} U_t^2$ can be neglected compared to $R_m g C_t \xi_{mp}$ in Eq. (18b). It then follows from Eq. (18b) that

$$R_m g C_t (\xi_{mp} - \xi_{ms}) = \frac{1}{2} U_{ts}^2 \tag{20a}$$

where ξ_{ms} denotes the value of ξ_m at the overflow point. Between Eqs. (19) and (20a), then,

$$\xi_{mp} = \xi_{ms} + \frac{1}{2} H_{ts} = \eta_{ts} + \frac{3}{2} H_{ts} = \eta_{ts} + \frac{3}{2} \left(\frac{q_{ws}^2}{R_m g C_t} \right)^{1/3} \tag{20b}$$

where η_{ts} denotes the elevation of the top of the barrier. The above condition allows for computation of the height of the interface at the point of basin overflow as a function of barrier elevation η_{ts}, outflow discharge per unit width q_{ws} and concentration C_t.

Sediment deposition within the basin

According to Eq. (12b) the suspended sediment concentration is not only constant in the vertical, but also constant in the streamwise direction, at least from the hydraulic jump to a point not far upstream of the downstream overflow point. In between these two zones, the rate of sediment deposition on the bed is given as $v_{sm} C_t$, implying that the deposit should consist of a pure drape of thickness that is constant in the streamwise direction. Solving Eq. (10) for a quasi-steady flow, deposit thickness is seen to vary in time as

$$\eta_t = \eta_{ti}(x) + \frac{v_{sm} C_t}{(1 - \lambda_{pm})} t \tag{21}$$

where $\eta_{ti}(x)$ denotes the initial profile of the bed.

The above theoretical solution applies only to the muddy pond. It does not locate the hydraulic jump relative to the barrier, nor does it describe the evolution of the topset and foreset upstream. In order to describe these features the theory must be embedded into a larger numerical framework. Before doing this, however, it is useful to introduce the results of an experiment that serve to justify several key assumptions made above.

Experiment

Experimental setup

An experiment was conducted in order to test both the above theoretical model, and a more complete numerical model. The experiment was carried out at St. Anthony Falls Laboratory, University of Minnesota. The experimental facility allows modeling of sustained turbidity of up to one hour (Garcia 1993). The flume is 0.304 m wide, 0.76 m deep and 12.80 m long, and has transparent glass walls. At the upstream end of the flume is a tank with a propeller that maintains a uniform water-sediment suspension, and also a damping tank at the downstream end, as sketched in Fig. 6. Normally the role of the damping tank is to prevent of reflection of turbidity currents from the downstream end of the flume. In the present experiment, however, a barrier placed a short distance upstream

of the invert to the damping tank played the role of the model dam (Fig. 6). This barrier, which had a nearly vertical face on the upstream side, caused reflection of the turbidity current as part of the process of setting up an internal hydraulic jump and quasi-steady ponded flow. Ambient water was impounded on both sides of the barrier, but was allowed to flow very slowly into the damping tank so as to maintain constant water surface elevation. That is, the experimental configuration reflected the geometry of Fig. 5b.

Only a reach of 7 m toward the downstream end of the flume was used for the experiments. A reservoir of simplified geometry illustrated in Fig. 6 was built in the flume. Its length was 5.8 m, and the maximum relief was 0.40 m. The initial bed in the central region of the reservoir was nearly horizontal with slope $S_b = 0.017$ ($\theta_b = 0.97^o$). A ski-jump configuration was located at the upstream end of the reservoir. Water and sediment were fed into the flume just upstream of the apex of ski-jump.

The above configuration is a simplification in that a) the ambient water did not spill over the barrier, as in a dam, but was impounded to the same elevation both sides, and b) no vent was provided, so that a ponded turbidity current could overflow only when the interface rises to an elevation ξ_m that is above the elevation of the top of the barrier η_{te} (but no higher than the water surface elevation ξ of impounded ambient water).

Water was supplied to the upstream end of the reservoir from the mixing tank shown in Fig. 6. The operation of the mixing tank is described in Toniolo et al. (in press(b)). Two grades of sediment were used: a black sand with a specific gravity of 2.60, a geometric mean size D_s of 500 μm and a geometric standard deviation of 1.47; and a white silt (mud) composed of glass beads with a specific gravity of 2.50, a geometric mean size D_m of 53 μm and a geometric standard deviation of 1.30. Denoting the submerged specific gravity of the sand as R_s, then, the corresponding values of R_s and R_m are 1.60 and 1.50. The grain size distributions of these two sediments are given in Fig. 7. Measurements of deposits yielded values of λ_{ps} and λ_{pm} of 0.40 and 0.42, respectively.

Black sand was delivered to the upstream end of the model reservoir with a screw feeder; white mud was first mixed to the desired concentration in the mixing tank and then pumped as a suspension to the upstream end of the model reservoir. The delivery rate of suspension from the mixing tank was controlled with a valve, and set to a specified value by means of repeated weighing of timed samples. The delivery rate of sand was controlled by a dial on the screw feeder.

Experimental procedure

The experiment was commenced with sediment-free water emanating form the mixing tank, into which black sand was mixed from the screw feeder. A well-defined fluvial topset and avalanching foreset formed and prograded into the reservoir. The foreset angle was close to 35°, i.e., the angle of repose of the black sand. Progradation continued until the toe of the foreset migrated well beyond the base of the ski jump shown in Fig. 6. In the absence of white mud only a thin bottomset formed.

Once the delta was established the mixing tank was filled with fresh water and a prescribed quantity of white mud (glass beads). The experiment was recommenced with a constant inflow of suspension from the mixing tank and black sand from the screw feeder. The volume discharge of the suspension and the feed rate of black sand were

adjusted to be equal to the respective values that prevailed in the absence of white mud. The flow continued in this way for 20 minutes, by which time the mixing tank was empty. The experiment was then temporarily halted, the mixing tank refilled with the suspension to the prescribed concentration and the run recommenced under identical conditions as before. The experiment was halted after three runs with input of the suspension, each with a duration of 20 minutes.

Measurements of suspended sediment concentration were performed in the experiment using 6 siphons. All but one of these siphons were members of one rake in which they were stacked vertically. This configuration allowed resolution of the vertical distribution of suspended sediment concentration. The distance downward from the water surface to each siphon was 3.5, 8.5, 18.5, 28.5, and 37.5 cm. The rake was mounted on a cart positioned at a point located 170 cm upstream of the barrier at the downstream end of the reservoir. The siphon farthest downstream was located at the lip of the downstream barrier. It served to quantify the outflow of sediment from the basin. Samples from each of the siphons were taken at several times during the experiment. At a given time, the sampling from all siphons was done simultaneously, so yielding a snapshot of the pattern of sediment suspension in the water column in the reservoir. These samples were analyzed to obtain sediment concentrations and grain size distributions. The distributions were determined using an Elzone particle counter device.

The water and slurry discharge was set equal to 1 l/s based on many previous trial numerical runs. The volume concentration, C_{ms} of white mud in the suspension was 2.5%, corresponding to a feed rate of 62.5 g/s. The feed rate of black sand was 9 g/s. The black sand thus constituted 12.6% of the incoming sediment by weight.

Experimental results

Profiles of bed deposits are shown in Fig. 8, in which the "initial bed" is in fact the bed at the end of the part of the experiment in which only black sand was supplied. Three other profiles are shown there, each corresponding to the end of a 20-minute period during which both black sand and white mud were supplied. The deposit thicknesses in the bottomset region are seen to be nearly constant, as predicted by Eq. (21).

The final bed deposit in the reservoir is shown in Fig. 9. Recalling that the black material is coarse and the white material is fine, the structure of the deposit is seen to be very similar to that observed in Lake Mead (Fig. 2). Although the topset is not shown, the foreset and bottomset are clearly visible. In addition, a substantial deposit of sediment can be seen downstream of the barrier. This confirms what was observed visually; in this experiment, the interface of the ponded zone was always located above the top of the barrier, so that substantial outflow of sediment was realized. The experiments of Toniolo et al. (in press(b)), however, confirm the possibility of an interface located below the top of the barrier, so that no sediment escapes.

The vertical profiles of volume sediment concentration at t = 20, 40, and 60 minutes from the commencement of the first run with slurry are presented in Fig. 10. The concentration profiles are approximately uniform in the vertical, indicating that the rake was located in the ponded zone downstream of the submerged hydraulic jump (Toniolo et al. in press(b)). The location of the interface between muddy and clear water is evidenced by the jump in concentration between the siphon located 3.5 cm below the water surface and the one located 8.5 cm below the water surface. The fact that the grain

size distribution was not absolutely uniform guaranteed the existence of a small amount of very fine sediment above an otherwise clear settling interface. A picture of this interface during the experiment is shown in Fig. 11, and an image showing the flow of turbid water over the downstream barrier is presented in Fig. 12. Figs. 10 and 11 provide approximate experimental confirmation of the assumption implicit in Eq. (6).

Fig. 13 shows plots of the vertical distributions of the geometric mean size obtained from the siphon samples during the experiment. This figure demonstrates the uniformity of the geometric mean size in the vertical. The longitudinal variation in the grain size distribution of the bottomset deposit at the end of the experiment was characterized by means of 11 bed samples. The grain sizes associated with the peaks of the probability densities of size are shown in Fig. 14. The peaks are used in preference to the geometric means due to the presence of small but unrealistic anomalies in the tails of the measured probability densities. Coarser beads were deposited in the fluvial topset and foreset. Nearly constant values of peak grain size were found along the bottomset to the barrier. The sediment deposited downstream of reservoir is seen to be slightly finer than that trapped in the reservoir.

Both black sand and the coarser sizes in the white mud deposited in the topset and foreset. On average 32.5 percent by weight of the topset consisted of white mud, the rest being black sand. With this in mind, the sediment size distributions and feed rates were re-partitioned into values reflecting the sediment deposited on the topset and foreset and values deposited on the bottomset. The effective size and feed rate for material deposited on the topset-foreset are 295 μm and 13.3 g/s (mostly black sand), and the corresponding values for material deposited on the bottomset are 49.7 μm and 58.14 g/s (all white mud). The above values are used as effective grain sizes and feed rates for "sand" and "mud" in the numerical model presented below.

Numerical Model

Definitions and assumptions

The formulation presented in the section "Theory for a Muddy Pond" provides an incomplete description of the experiment of the previous section in that it a) does not locate the hydraulic jump relative to the barrier, and b) does not describe the co-evolving topset, foreset, and bottomset of the deposit, as well as the fluvial and turbidity current flows that emplace these features. The theory must be embedded in a larger framework and solved numerically to capture these features. Here the delta model of Kostic and Parker (2003(a), 2003(b)) is used as the basis for this extension.

Let $x = 0$ now denote the origin at which water and sediment are introduced, and $x = s_s(t)$, $s_p(t)$ and $s_b(t)$ denote the positions of three moving boundaries, i.e., the topset-foreset break (shoreline), plunge point and foreset-bottomset break, respectively (Fig. 1). In addition, $x = s_d$ denotes the fixed position of the downstream barrier (dam). The topset extends from $x = 0$ to $x = s_s(t)$, the foreset extends from $x = s_s(t)$ to $x = s_b(t)$ and the bottomset extends from $x = s_b(t)$ to $x = s_d$.

The positions of the topset-foreset intersection and the foreset-bottomset intersection are denoted correspondingly as (η_s, s_s) and (η_b, s_b). The slope of the foreset is denoted as S_a. Both S_a and water surface elevation ξ are assumed constant here, a condition that can be easily relaxed (see the Appendix of Kostic and Parker, 2003(a)).

The barrier at $s = s_d > s_b$, is assumed to be vertical and to allow overflow. The elevation of the muddy pond may be below or above the lip of the barrier.

The sediment is abstracted to two sizes; a sand size D_s and a mud size D_m; the volume sand and mud discharges per unit width are denoted as q_s and q_m, respectively. Constant water discharge per unit width q_{wf}, sand discharge per unit width q_{so} and mud discharge per unit width q_{mo} are supplied at $x = 0$. The sand (but no mud) deposits entirely in the topset and foreset. The mud is carried through the fluvial zone as wash load. The muddy water then plunges in the vicinity of the foreset to form a purely depositional turbidity current that emplaces a bottomset composed purely of mud. Because of the assumption of a constant width the river flow upstream of the foreset is treated using the 1D St. Venant equations of shallow water flow, and the turbidity current downstream of the foreset is treated using the corresponding 1D layer-averaged relations for a turbidity current.

Relations for the fluvial topset region

The quasi-steady approximation (de Vries 1965) is employed in this region. The equations governing fluvial flow are

$$U_f H_f = q_{wf}$$

$$\frac{d}{dx}(U_f^2 H_f) = -gH_f \frac{dH_f}{dx} + gH_f S_f - C_{fa} U_f^2 \qquad (22, 23)$$

where q_{wf}, U_f and H_f = (constant) water discharge per unit width, streamwise depth-averaged flow velocity and depth in the fluvial region, respectively S_f = bed slope given by the relation

$$S_f = -\frac{d\eta_f}{dx} \qquad (24)$$

where η_f = bed elevation in the fluvial region, and C_{fa} denotes the friction coefficient for the subaerial (fluvial) region, here assumed constant for simplicity. The local boundary shear stress τ_b in the fluvial region is given by the relation

$$\tau_b = \rho C_{fa} U_f^2 \qquad (25)$$

Eqs. (22) and (23) can be reduced to the backwater forms

$$U_f = \frac{q_w}{H_f}$$

$$\frac{dH_f}{dx} = \frac{S_f - S_{fr}}{1 - \boldsymbol{Fr}^2} \qquad (26, 27)$$

where

$$\boldsymbol{Fr} = \frac{U_f}{\sqrt{gH_f}} \qquad S_{fr} = C_{fa} \boldsymbol{Fr}^2 \qquad (28, 29)$$

In the above relations $\boldsymbol{Fr}$ denotes the Froude number of open-channel flow (rather than the densimetric Froude number of a turbidity current) and S_{fr} denotes the friction slope. The fluvial flow is assumed to be subcritical i.e., $\boldsymbol{Fr} < 1$. The boundary condition on Eq. (27) is thus a specified depth H_f at $x = s_s$, i.e.

$$H_f\big|_{s_s} = H_s \equiv \xi - \eta_s \qquad (30)$$

where ξ denotes the (constant) water surface elevation in the reservoir.

The Exner equation of bed sediment continuity on the fluvial region is

$$(1-\lambda_{ps})\frac{\partial \eta_f}{\partial t} = -\frac{\partial q_s}{\partial x} \tag{31}$$

where λ_{ps} = porosity of the sand deposit. A generalized sediment transport relation of the following form is assumed for the bed-material transport of sand;

$$q^* = \alpha\left(\tau^* - \tau_c^*\right)^n \tag{32a}$$

where α and n are specified parameters, q^* and τ^* denote the Einstein and Shields numbers, respectively defined as

$$q^* = \frac{q_s}{\sqrt{R_s g D_s} D_s} \qquad \tau^* = \frac{\tau_b}{\rho R_s g D_s} \tag{32b, c}$$

The parameter τ_c^* in Eq. (32a) denotes a critical Shields stress for the onset of motion. The total bed material load relation of Engelund and Hansen (1972) used here is realized for the choices

$$\alpha = \frac{0.05}{C_{fa}} \qquad n = 2.5 \qquad \tau_c^* = 0 \tag{33a, b, c}$$

In the present analysis bedforms are assumed to be absent in the fluvial zone, so that the boundary shear stress consists solely of skin friction. Generalization so as to include form drag due to bedforms in the resistance and sediment transport formulations is relatively straightforward.

Eq. (31) must be solved subject to a) an initial condition, here specified as a bed with a constant slope S_{fbi}, b) a specified upstream sand feed rate q_{so} at $x = 0$ and c) a shock condition at the foreset as specified below.

Relations for the turbidity current (subaqueous) region

It is assumed that the flow plunges at point $x = s_p$ just beyond the top of the foreset, so forming a mud-laden turbidity current. The turbidity current region extends from $x = s_p$ to $x = s_d$. The volume transport rate per unit width of mud by the turbidity current is q_m, where

$$q_m = U_t H_t C_t \tag{34}$$

The turbidity current is assumed to be diluted in the sense that $C_t << 1$.

The equations governing the turbidity current region must describe the turbidity current both upstream and downstream of the hydraulic jump to a muddy pond. With this in mind, Eqs. (7), (9) and (11) are generalized to the forms

$$\frac{\partial H_t}{\partial t} + \frac{\partial U_t H_t}{\partial x} = (1-\delta) e_w U_t - \delta v_{sm}$$

$$\frac{\partial C_t H_t}{\partial t} + \frac{\partial U_t C_t H_t}{\partial x} = -r_o v_{sm} C_t \tag{35a, b, c}$$

$$\frac{\partial U_t H_t}{\partial t} + \frac{\partial U_t^2 H_t}{\partial x} + \delta U_t v_{sm} = -\frac{1}{2} R_m g \frac{\partial C_t H_t^2}{\partial x} + R_m g C_t H_t S_t - C_{fs} U_t^2$$

where e_w is a dimensionless coefficient of water entrainment from the ambient fluid above, C_{fs} is a dimensionless coefficient of bottom friction of the turbidity current, here assumed constant for simplicity and r_o is a dimensionless coefficient relating near-bed

mud concentration to layer-averaged mud concentration C_t. In addition, δ is a parameter taking the value 0 in a Froude-supercritical turbidity current without a settling interface and the value 1 in a highly subcritical Froude-subcritical turbidity current with a clear settling interface. The effect of detrainment is realized for the case $\delta = 1$. The coefficient of water entrainment from above is given by the following relation proposed by Parker et al. (1986);

$$e_w = \frac{0.00153}{0.0204 + \boldsymbol{Ri}} \tag{36}$$

where ***Ri*** denotes the bulk Richardson number, related to the densimetric Froude number as

$$\boldsymbol{Ri} = \frac{1}{\boldsymbol{Fr}_d^2} \tag{37}$$

The formulation of Eqs. (35a) and (35c) includes the *ad-hoc* parameter δ characterizing detrainment. In a more formal derivation δ would vary smoothly from 0 to 1 as the flow ranges from highly supercritical to highly subcritical. The presence of a jump to highly subcritical flow allows use of the approximate formulation here. The justification of the detrainment terms was given in the section "Theory for a Muddy Pond".

Eq. (35b) dictates that the turbidity current is purely depositional, with no entrainment of sediment from the bed. The fall velocity v_{sm} is computed from the relation of Dietrich (1982).

It is important to note that while Eqs. (22) and (23) of the fluvial region are in quasi-steady form, Eqs. (35a, b, c) of the turbidity current region retain the time derivative terms. The retention of these terms and the conservative form of Eqs. (35a, b, c) allow for shock-capturing of any migrating bore or internal hydraulic jump that forms within the solution domain. In accordance with the work of Wilkinson and Wood (1971) Stefan and Hayakawa (1972) and Baddour (1987) the entrainment of ambient water by any internal hydraulic jump is neglected.

In the turbidity current region the Exner equation of sediment continuity takes a slightly generalized form of Eq. (10);

$$(1-\lambda_{pm})\frac{\partial \eta_t}{\partial t} = r_o v_{sm} C_t \tag{38}$$

Plunging is assumed to occur within the foreset domain $s_s < s_p < s_b$, so that the turbidity current flows down a portion of the relatively steep foreset before reaching the more gently-sloping bottomset (Fig. 1). Over the domain $s_p < x < s_b$ it is assumed that the turbidity current is too swift to deposit mud on the foreset, but not competent to entrain sand from it, so that within only this limited domain Eqs. (35b) and (38) are modified to the respective forms

$$\frac{\partial C_t H_t}{\partial t} + \frac{\partial U_t C_t H_t}{\partial x} = 0$$
$$(1-\lambda_{pm})\frac{\partial \eta_t}{\partial t} = 0 \tag{39a, b}$$

Shock condition across the foreset

The Exner equation of mass continuity of sand, Eq. (31), may be integrated across the foreset to yield the shock relation

$$(1-\lambda_{ps})\int_{s_s}^{s_b}\frac{\partial \eta}{\partial t}dx = -\int_{s_s}^{s_b}\frac{\partial q_s}{\partial s}dx \tag{40}$$

(Swenson et al. 2000; Kostic and Parker 2003(a), 2003(b)). The boundary condition at the base of the foreset is that of vanishing sand load, i.e.

$$q_s\big|_{s_b} = 0 \tag{41}$$

The bed profile across the foreset domain $s_s < x < s_b$ is given as

$$\eta = \eta_s - S_a(x - s_s) \tag{42}$$

where S_a denotes the slope of avalanching of the foreset, here assumed to be a specified constant and

$$\eta_s \equiv \eta_f[s_s(t),t] \tag{43}$$

Thus between Eqs. (42) and (43), the following condition prevails on the foreset;

$$\frac{\partial \eta}{\partial t} = \frac{\partial \eta_f}{\partial t}\bigg|_{s_s} - S_{fs}\dot{s}_s + S_a\dot{s}_s \qquad S_{fs} = -\frac{\partial \eta_f}{\partial x}\bigg|_{S_s} \tag{44a, b}$$

where the dot denotes a derivative in time. The foreset shock condition is found between Eqs. (40), (41) and (44a, b) to be

$$(s_b - s_s)\left[\frac{\partial \eta_f}{\partial t}\bigg|_{s_s} + (S_a - S_{fs})\dot{s}_s\right] = \frac{q_{ss}}{(1-\lambda_{ps})} \qquad q_{ss} \equiv q_s\big|_{s_s} \tag{45a, b}$$

Eq. (45a) provides a condition for determining the speed of progradation of the topset-foreset break $\dot{s}_s$ as a function of the volume rate of sand delivery per unit width q_{ss} to the topset-foreset break and the foreset geometry.

Condition for plunging

The conditions for plunging are illustrated in Fig. 1. Because flow depth increases strongly in the streamwise direction on the foreset, it is assumed that the mud-laden flow plunges over it. Water surface elevation is assumed to be constant and equal to ξ for $x \geq s_s$. Flow depth H_f on the foreset is thus given as

$$H_f = H_s + S_a(x - s_s) \qquad H_s = \xi - \eta_s \tag{46a, b}$$

Local densimetric Froude number $\boldsymbol{Fr}_d$ and bulk Richardson number $\boldsymbol{Ri}$ on the foreset before plunging are given from Eqs. (1), (34) and (37) (but with the transformation $U_t \rightarrow U_f$ because the muddy flow has not plunged yet);

$$\boldsymbol{Fr}_d^2 = \frac{q_{wf}^3}{R_m g q_{mo} H_f^3} \qquad \boldsymbol{Ri} = \boldsymbol{Fr}_d^{-2} \tag{47a, b}$$

where q_{mo} denotes the volume rate of feed of mud per unit width, which is also equal to the volume mud discharge per unit width at the topset-foreset break.

Plunging is computed using a modified version of the formulation of Akiyama and Stefan (1984) given in Parker and Toniolo (submitted). As the river flow plunges on the foreset to form a turbid underflow, it tends to entrain ambient water from the reservoir, thus increasing its forward discharge per unit width above the river value q_w. This entrainment can be characterized in terms of a dimensionless mixing coefficient γ defined in the following way;

$$U_{tp}H_{tp} = q_{wf}(1+\gamma) \tag{48}$$

where U_{tp} and H_{tp} denote the layer-averaged flow velocity and layer thickness of the turbid underflow just after plunging. The formulation of Parker and Toniolo (submitted) allows computation of both the densimetric Froude number just before plunging $\boldsymbol{Fr}_{dp}$ and the ratio

$$\varphi = \frac{H_{tp}}{H_{fp}} \tag{49}$$

where H_{fp} denotes the depth of river flow on the foreset just before plunging, as functions of γ. Here the value of γ is determined by calibration to the experiments, and $\boldsymbol{Fr}_{dp}$ is computed from Fig. 2 of Parker and Toniolo (submitted). Once $\boldsymbol{Fr}_{dp}$ is known the value of H_{fp}, and thus the plunge point s_p can be computed from Eqs. (47a) and (46a), or equivalently

$$H_{fp} = \left(\frac{q_{wf}^3 \boldsymbol{Ri}_{fp}}{R_m g q_{mo}} \right)^{1/3} \qquad s_p = s_s + \frac{H_{fp} - H_s}{S_a} \qquad \boldsymbol{Ri}_{fp} = \boldsymbol{Fr}_{dp}^{-2} \tag{50a, b, c}$$

The values of H_{tp} and U_{tp} are then obtained from the predicted value of φ, and Eqs. (47a) and (48), respectively. The value C_{tp} of the volume concentration of sediment in the turbidity current just after plunging is given by another relation in Parker and Toniolo (submitted), which takes the form

$$C_{tp} = \frac{q_{mo}}{q_{wf}(1+\gamma)} \tag{50d}$$

A necessary condition for plunging on the foreset is that

$$s_s < s_p < s_b \tag{51}$$

The analysis can, however, be modified for the case of a turbidity current that plunges beyond the toe of the foreset.

Upstream boundary conditions on the turbidity current are thus determined based on values on the downstream side of the plunge point;

$$H_t\big|_{s_p} = H_{tp} \qquad U_t\big|_{s_p} = U_{tp} \qquad C_t\big|_{s_p} = C_{tp} \tag{52a, b, c}$$

Condition for movement of the foreset-bottomset interface

The position of the foreset-bottomset break is (η_b, s_b). Here (η_b, s_b)and (η_s, s_s) are related as

$$\eta_b = \eta_s - S_a(s_b - s_s) \tag{53}$$

Recall that η_s is defined in Eq. (43); the corresponding definition for η_b is

$$\eta_b \equiv \eta_t[s_b(t), t] \tag{54}$$

Taking the time derivative of both sides of Eq. (54) and evaluating the time derivative of η_b in the same way as was done for that of η_s between Eqs. (43) and (44), it is found that

$$\left.\frac{\partial \eta_t}{\partial t}\right|_{s_b} - S_{tb}\dot{s}_b = \left.\frac{\partial \eta_f}{\partial t}\right|_{s_s} - S_{fs}\dot{s}_s - S_a(\dot{s}_b - \dot{s}_s) \tag{55a}$$

where

$$S_{tb} = -\left.\frac{\partial \eta_t}{\partial x}\right|_{s_b} \tag{55b}$$

Boundary conditions at the barrier

As long as the flow in the ponded zone of the turbidity current is highly subcritical, the elevation of the settling interface ξ_m (sufficiently upstream of the barrier if there is any overflow) is given as ξ_{mp}, where

$$\xi_{mp} = \left(\eta_t + H_t\right)\Big|_{ponded\ zone} \tag{56}$$

can be expected to be nearly horizontal, and the value of U_t can be expected to be very low. The nature of the boundary condition at the dam changes depending on whether ξ_{mp} is below or above an outflow barrier, as described in Fig. 5b. In the former case the downstream boundary condition at the dam is simply

$$U_t\Big|_{x=s_d} = 0 \tag{57}$$

In the latter case the turbidity current is assumed to reach a densimetric Froude number of unity over the barrier, according to Eq. (19); the downstream boundary condition is then given as

$$H_t\Big|_{x=s_d} = \frac{U_t^2\Big|_{x=s_d}}{R_m g C_t\Big|_{x=s_d}} \tag{58}$$

The numerical model in its present form cannot continuously encompass the progression from a no-overflow condition to an overflow condition. As a result the model is run using Eq. (57) as the downstream boundary condition, but with a barrier elevation increased arbitrarily from η_{ts} to $\eta_{ts} + \Delta\eta$, where $\Delta\eta/\eta_{ts} << 1$. Once ξ_{mp} rises to the level $\eta_{te} + \Delta\eta$, the model is continued using the overflow condition of Eq. (58) and the original barrier height η_{ts}.

Transformation to moving boundary coordinates

A transformation to moving-boundary coordinates allows for explicit tracking of the position of the delta front as the calculation proceeds (Swenson et al. 2000). The following transformation is made on the topset fluvial zone $0 < x < s_s$:

$$\hat{t}_f = t \qquad \hat{s}_f = \frac{x}{s_s} \tag{59a, b}$$

It follows that

$$\frac{\partial}{\partial t} = \frac{\partial}{\partial \hat{t}_f} - \hat{s}_f \frac{\dot{s}_s}{s_s}\frac{\partial}{\partial \hat{s}_f} \qquad \frac{\partial}{\partial x} = \frac{1}{s_s}\frac{\partial}{\partial \hat{s}_f} \tag{60a, b}$$

The corresponding transformation for the bottomset turbidity current zone $s_b < x < s_d$ is

$$\hat{t}_t = t \qquad \hat{s}_t = \frac{x - s_b}{s_d - s_b} \tag{61a, b}$$

from which

$$\frac{\partial}{\partial t} = \frac{\partial}{\partial \hat{t}_t} - \frac{\dot{s}_b(1 - \hat{s}_t)}{s_d - s_b}\frac{\partial}{\partial \hat{s}_t} \qquad \frac{\partial}{\partial x} = \frac{1}{s_d - s_b}\frac{\partial}{\partial \hat{s}_t} \tag{62a, b}$$

In the fluvial zone, Eqs. (27), (31), (30) and the condition of specified sand supply rate q_{so} at $x = 0$ transform as follows;

$$\frac{dH_f}{d\hat{s}_f} = \frac{S_f - S_{fr}}{1 - \boldsymbol{Fr}^2} s_s \tag{63}$$

$$(1-\lambda_{ps})\left(\frac{\partial \eta_f}{\partial \hat{t}_f}-\hat{s}_f\frac{\dot{s}_s}{s_s}\frac{\partial \eta_f}{\partial \hat{s}_f}\right)=-\frac{1}{s_s}\frac{\partial q_s}{\partial \hat{s}_f} \tag{64}$$

$$H_f\Big|_{\hat{s}_f=1}=\xi-\eta_s \quad , \quad q_s\Big|_{\hat{s}_f=0}=q_{so} \tag{65a, b}$$

In the bottomset turbidity current zone, Eqs. (35a-35c) take the moving-boundary forms

$$\begin{aligned}
&\frac{\partial H_t}{\partial \hat{t}_t}-\frac{\dot{s}_b(1-\hat{s}_t)}{s_d-s_b}\frac{\partial H_t}{\partial \hat{s}_t}+\frac{1}{s_d-s_b}\frac{\partial U_t H_t}{\partial \hat{s}_t}=(1-\delta)e_w U_t-\delta v_{sm}\\
&\frac{\partial C_t H_t}{\partial \hat{t}_t}-\frac{\dot{s}_b(1-\hat{s}_t)}{s_d-s_b}\frac{\partial C_t H_t}{\partial \hat{s}_t}+\frac{1}{s_d-s_b}\frac{\partial U_t C_t H_t}{\partial \hat{s}_t}=-r_o v_{sm} C_t\\
&\frac{\partial U_t H_t}{\partial \hat{t}_t}-\frac{\dot{s}_b(1-\hat{s}_t)}{s_d-s_b}\frac{\partial U_t^2 H_t}{\partial \hat{s}_t}+\frac{1}{s_d-s_b}\frac{\partial U_t^2 H_t}{\partial \hat{s}_t}+\delta U_t v_{sm}=\\
&-\frac{1}{2}\frac{R_m g}{s_d-s_b}\frac{\partial C_t H_t^2}{\partial \hat{s}_t}+R_m g C_t H_t S_t-C_{fs}U_t^2
\end{aligned} \tag{66a, b, c}$$

The upstream boundary conditions on the above relations are

$$U_t\Big|_{\hat{s}_t=0}=U_{to} \qquad H_t\Big|_{\hat{s}_t=0}=H_{to} \qquad C_t\Big|_{\hat{s}_t=0}=C_{to} \tag{67a, b, c}$$

where U_{to} and H_{to} are computed by solving Eqs. (35a), (35c) and (39a) from the plunge point to the foreset-bottomset break under the assumption of no exchange of sediment with the bed along the steep foreset. Eqs. (38), (45a) and (55a) takes the moving-boundary forms

$$(1-\lambda_{pm})\left(\frac{\partial \eta_t}{\partial \hat{t}_t}-\frac{\dot{s}_b(1-\hat{s}_t)}{s_d-s_b}\frac{\partial \eta_t}{\partial \hat{s}_t}\right)=r_o C_t \tag{68}$$

$$\dot{s}_s=\frac{1}{S_a}\left[-\frac{\partial \eta_f}{\partial \hat{t}_f}\Big|_{\hat{s}_f=1}+\frac{1}{s_b-s_s}\frac{q_{ss}}{(1-\lambda_{ps})}\right] \tag{69}$$

$$\dot{s}_b=\dot{s}_s+\frac{1}{S_a}\left(\frac{\partial \eta_f}{\partial \hat{t}_f}\Big|_{\hat{s}_f=1}-\frac{\partial \eta_t}{\partial \hat{t}_t}\Big|_{\hat{s}_t=0}\right) \tag{70}$$

The downstream boundary conditions described by Eqs. (57) and (58) transform to the respective forms

$$U\Big|_{\hat{s}_t=1}=0 \quad , \quad H_t\Big|_{\hat{s}_t=1}=\frac{U_t^2\Big|_{\hat{s}_t=1}}{R_m g C_t\Big|_{\hat{s}_t=1}} \tag{71, 72}$$

Implementation

In implementing the numerical model, the parameters q_{wf}, q_{so}, q_{mo}, R_s, R_m, λ_{ps}, λ_{pm}, v_{sm}, r_o, C_{fa}, C_{fs}, η_{ts}, s_d, S_a, γ, η_{ts}, D_m and D_s must be specified by the user. In addition, appropriate initial conditions for the bed must be prescribed; these are done here in terms of specified initial values of bed slope on the topset fluvial region S_{fi}, bed slope on the

bottomset region S_{ti}, distance to the topset-foreset break s_{si}, elevation at the topset-foreset break η_{si} and elevation at the foreset-bottomset break η_{bi}.

The fluvial model is implemented as follows. First Eq. (63) is solved upstream of the point $\hat{s}_f = 1$ over a known bed using the boundary condition of Eq. (65a) and a standard step method. Once the depth H_f is known everywhere, q_s is evaluated using Eqs. (32) and (25), and $\dot{s}_s$ is computed from Eq. (69). The time derivative in Eq. (69) may be brought in iteratively, or evaluated based on the results of the previous time step. The new bed one time step later is the computed using an explicit scheme applied to Eq. (64) subject to the boundary condition of Eq. (65b), which is enforced at a ghost node one step upstream of the origin.

The turbidity current is calculated rather differently. The necessity of capturing the hydraulic jump requires the use of a technique that does not employ the quasi-steady assumption; that is, the time derivatives in Eqs. (66a, b, c) are not dropped here. These equations are in conservative form, which means that any hydraulic jump is automatically captured.

Starting from a given bed and quite arbitrary initial conditions on the flow, Eqs. (66a, b, c) are solved numerically using a MacCormack scheme (MacCormack 1969; Tannehill et al. 1997) subject to the boundary conditions of Eqs. (67a, b, c) upstream and either Eq. (71) or Eq. (72) downstream (the choice of which must be made by trial and error). Such a scheme automatically captures, where appropriate, the formation of a turbidity current with a distinct head, the collision of the head with the dam, reflection producing an upstream-migrating bore, and eventual stabilization to a steady flow with a hydraulic jump. The achievement of this steady flow is very rapid in terms of the characteristic time for morphologic evolution.

The steady solution so obtained is in fact only quasi-steady, because the bed is evolving at a time scale that is much slower than that required for setup of the flow. The quasi-steady solution is then substituted into Eqs (68) and (70) to compute bed evolution and the speed of migration $\dot{s}_b$ of the foreset-bottomset break. The time derivatives in Eq. (70) may be brought in iteratively, or evaluated based on the results of the previous time step.

Numerical Simulation of the Experiment

The numerical model was tested against the results of the above experiment. The following parameters were used in the model; q_{wf} =0.00353 m^2/s (corresponding to 1 l/s), q_{so} = 1.68 x10^{-5} m^2/s (13.3 g/s), q_{mo} =7.60 x10^{-5} m^2/s (58.1 g/s), R_s = 1.60, R_m = 1.50, λ_{ps} = 0.40, λ_{pm} = 0.42, D_m =49 μm, r_o = 1, D_s = 295 μm, S_a =0 .64, s_d = 5.80 m, s_{si} = 0.5 m, ξ = 10.04 m, η_{bi} = 9.645 m, η_{ts} = 10.03 m, S_{fi} =0.02 and S_{ti} = 0.0167. The parameters C_{fa}, C_{fs} and γ were calibrated to the experiment; the values so obtained were as follows;

$$C_{fa}^{-1/2} = 8 \quad , \quad C_{fs}^{-1/2} = 30 \quad , \quad \gamma = 1.3 \qquad \text{(73a, b, c)}$$

The calculation proved to be not particularly sensitive to the choices of C_{fa} and C_{fs}, but much more sensitive to the choice of γ.

The results of the simulation of the experiment are shown in Fig. 15 for bed and interface profiles and Fig. 16 for time evolution of the foreset-bottomset break. A comparison of Fig. 15 with Fig. 8 shows that the model provides a good simulation of the evolution of the bed. In addition, it is seen from Fig. 15 that the model correctly predicts

the turbidity current as overflowing the barrier, as observed in Fig. 12. More specific verification is given in Fig. 17, which shows measured and simulated profiles for deposit thickness at t = 60 min; the agreement is good.

Field-scale Simulation

The numerical model was applied to a hypothetical reservoir at field scale. The geometric characteristics are as follows: the length s_d is 6000 m and the initial length of fluvial zone (i.e, s_{si}) is 1000 m. The initial topset and bottomset bed slopes S_{fi} and S_{ti} are 0.00073 and 0.016 respectively. The initial elevations of the top and bottom of the foreset η_s and η_b are as 200 m and 100 m, respectively. The foreset slope S_a is set equal to 0.2 (11.3°). The elevation η_{ts} of the top of the barrier at the downstream end of the reservoir is 165 m, and the water surface elevation in the reservoir is fixed at 203 m. Neither orifices nor gates are considered at the downstream end, so that any outflow of turbid water passes over the barrier. As in the case of the experiment, ambient water is impounded to a constant elevation ξ, on both sides of the barrier.

The fluvial water discharge per unit width q_{wf} for the simulation is 2 m^2/s. The dimensionless Chezy resistance coefficients $C_{fa}^{-1/2}$ and $C_{fs}^{-1/2}$ for the subaerial (topset) and subaqueous (bottomset) regimes are set to 12 and 30 respectively. The simulation uses sand with D_s= 400 μm, R_s= 1.65, and λ_{ps}= 0.4 and mud with D_s= 50 μm, R_s= 1.65, and λ_{pm}= 0.6. The input rates q_{so} and q_{mo} of sand and mud are 6.25 x 10^{-4} m^2/s and 6.25 x 10^{-3} m^2/s, respectively.

The total run time is 90 days of continuous flood flow, which easily translates into years or decades of real time. The geomorphic time step, i.e., that used in Eqs. (64) and (68), is 2 h. The fluvial and subaqueous regions are divided into 94 nodes each. In running the turbidity current model, $\Delta\eta$ was set equal to 1 m.

Figs. 18, 19, and 20 illustrate the predictions of the model. Fig. 18 shows the evolution of the bed profile in time. The final profile of the turbidity current interface, showing the hydraulic jump and the ponded zone is included. The gradual filling of the reservoir as the foreset progrades and the bottomset builds up is clearly documented.

Fig. 19 shows the time variation of the interface between muddy and clear water in the ponded zone. Also shown is the elevation of the barrier at the downstream end. It is seen that no overflow occurs until t = 15 days. After this time the turbidity current overflows the barrier and sediment escapes.

Fig. 20 shows the time variation of the trap efficiency of the reservoir. The trap efficiency is 100 percent up to t = 15 days, during which time the interface of the muddy pond lies below the top of the barrier. Beyond that time the trap efficiency is seen to gradually decrease in time as increasingly larger amounts of sediment spill out.

Discussion

The model presented here captures the formation and progradation of the topset and foreset, as well as the buildup of the bottomset in a reservoir. It captures plunging and the formation of a depositional turbid underflow, as well as the internal hydraulic jump and muddy pond farther downstream. Most importantly, it captures the process of detrainment of water from the muddy pond, a phenomenon which if sufficiently strong can prevent any overflow of turbid water. As such, it captures the essence of the mechanics behind the Brune (1953) diagram for reservoir trap efficiency.

The formulation has a number of limitations. Real reservoirs, as well as their deltas at the upstream end, have 2D rather than 1D geometries. Bottom vents have not been specifically included in the analysis. Real reservoirs are bounded at the downstream end by an impoundment permitting the overspill of water, sediment-free or otherwise, not a submerged barrier. These limitations are of a purely technical nature, and can be overcome using existing techniques of numerical modeling.

More problematical is the limitation to a single size for sand and a single size for mud. River mud in particular is usually poorly sorted, and as such can be expected to form multiple settling interfaces in the ponded zone. The formulation needs to be extended to multiple mud sizes and multiple settling interfaces.

Attention to the above points will place a predictive model of reservoir sedimentation and trap efficiency within the reach of the practicing engineer.

Conclusions

The simplified 1D model presented here represents a first but important step toward a numerical model capable of predicting reservoir trap efficiency. It describes the physics of a) fluvial deposition of sand on the delta topset, b) progradation of the foreset due to sand deposition, c) plunging of muddy river water to form a bottom turbidity current, d) the formation of an internal hydraulic jump and a muddy pond downstream due to the presence of the dam, e) deposition of mud from the turbidity current to form the bottomset, and most importantly f) the detrainment of water across the settling interface of the muddy pond.

The effect of detrainment is to sap the forward discharge of the ponded turbidity current. If detrainment is sufficiently large, the discharge of the turbidity current drops to zero at the dam, and the interface falls below any overflow point. This yields a sediment trap efficiency of 100 percent. In time, however, buildup of the bottomset and progradation of the foreset guarantee that the settling interface must eventually rise above a point of overflow, after which the trap efficiency of the reservoir gradually declines. As such, the model contains the physics to move beyond the Brune (1953) diagram in explaining and predicting reservoir sedimentation.

Acknowledgments

This research was partially funded by the Office of Naval Research STRATAFORM program. It was also partially funded by the National Center for Earth-surface Dynamics (NCED), which is in turn funded by the Science and Technology Centers (STC) program of the National Science Foundation. This paper represents a contribution to the NCED effort on river restoration.

Notation

The following symbols are used in this paper:

A	=	cross-sectional area of a cylinder
B_r	=	width of the reservoir
C_{ms}	=	volume concentration of white silt in the mixing tank.
C_{fa}	=	bed friction coefficient for the subaerial (fluvial) region
C_{fs}	=	dimensionless coefficient of bottom friction for the turbidity current

C_t = layer-averaged volume concentration of mud in a turbidity current
C_{to} = value of C_t at the foreset-bottomset break
C_{tp} = value of C_t just after plunging
c = volume concentration of mud in the turbidity current
D_s, D_m = characteristic grain size of sand and mud, respectively
e_w = mixing coefficient of ambient water into the turbidity current
$\boldsymbol{Fr}$ = Froude number of open-channel flow
$\boldsymbol{Fr_d}$ = densimetric Froude number of turbidity current
$\boldsymbol{Fr_{dp}}$ = densimetric Froude number just after plunging
g = acceleration of gravity
H_{fp},H_{tp} = fluvial depth just before and turbidity current thickness just after plunging
H_f = depth in the fluvial region
H_s = river depth at the topset- foreset break
H_t = layer thickness of turbidity current
H_{to} = value of H_t at the foreset-bottomset break
H_{ts} = value of H_t over the barrier (sill)
n = exponent in the sand transport relation
L_p = length of the ponded zone in the reservoir
L_r = length of the reservoir
Q_d = detrainment discharge
Q_j = flow discharge just downstream of the hydraulic jump
q_m, q_s = volume transport rate per unit width of mud and sand, respectively
q_{mo}, q_{so} = volume transport rate per unit width of mud and sand at $x = 0$
q_{ss} = volume transport rate per unit width of sand at the topset-foreset break
q^* = Einstein number characterizing dimensionless sand transport rate
q_{wf} = (constant) water discharge per unit width on the fluvial region
q_w = flow discharge per unit width of the turbidity current
q_{wj}, q_{ws} = value of q_w just after the hydraulic jump; value of q_w overflowing the barrier (sill)
$\boldsymbol{Ri}$ = bulk Richardson number
$\boldsymbol{Ri_{fp}}$ = fluvial bulk Richardson number just after plunging
R_m = $= (\rho_{sm}/\rho - 1)$, submerged specific gravity of mud
R_s = $= (\rho_{ss}/\rho - 1)$, submerged specific gravity of sand
r_o = coefficient relating near-bed volume suspended sediment concentration c_b to the layer-averaged value C_t, such that $c_b = r_o C_t$
S_a = foreset slope
S_b = reservoir bottom slope
S_{bi} = initial reservoir bottom slope
S_f = bed slope on the fluvial region
S_{fi} = initial bed slope on the fluvial region
S_{fs} = bed slope on the fluvial region at the topset-foreset break
S_{fr} = friction slope in fluvial region
S_t = bed slope in the turbidity current region (reservoir)

S_{ti} = initial bed slope in the turbidity current region (reservoir)
S_{tb} = bottomset bed slope at the foreset-bottomset break
s_b, s_d, = location of the foreset-bottomset break and dam
s_p, s_s = location of the plunge point and topset-foreset break
s_{si} = initial location of the topset-foreset break
$\dot{s}_b$, $\dot{s}_s$ = speed of migration of the foreset-bottomset break; speed of migration of the topset-foreset break
$\hat{s}_f$, $\hat{s}_t$ = streamwise moving boundary coordinates in the fluvial and turbidity current regions, respectively
t = time
$\hat{t}_f$, $\hat{t}_t$ = time in the fluvial moving boundary formulation; time in the moving boundary coordinate formulation for the turbidity current region
U_f, U_t = streamwise layer-averaged flow velocity in the fluvial region; streamwise layer-averaged flow velocity in the turbidity current region
U_{to} = value of U_t at the base of the topset-foreset break
U_{tp} = value of U_t just after plunging
U_{ts} = value of U_t over the barrier (sill)
u = streamwise flow velocity of turbidity current
v = upward normal flow velocity of turbidity current
v_{sm} = fall velocity of mud
x = bed-attached streamwise coordinate
y = bed-attached upward normal coordinate
α = coefficient in the sand transport relation
δ = parameter equal to unity in the subcritical (ponded) zone and zero in the supercritical zone upstream of the internal hydraulic jump
γ = mixing coefficient associated with plunging
Δh = reservoir relief from the bed elevation at the base of the dam to the lowest overflow point.
$\Delta\eta$ = small elevation difference used in calculation transition to overflow at the downstream barrier
η = bed elevation
η_b, η_f, = bed elevation at the foreset-bottomset break and bed elevation on the fluvial region
η_{bi} = initial elevation at the foreset-bottomset break
η_s = bed elevation at the topset-foreset break
η_t, η_{ti}, = bed elevation in the reservoir and initial bed elevation in the reservoir
η_{te} = elevation of the top of the barrier (sill)
η_{ts} = bed elevation of the top of the barrier (sill)
φ = ratio of downstream turbidity current thickness to upstream flow depth at plunge point
λ_{pm} = mud porosity

λ_{ps}	=	sand porosity
θ_b	=	angle
ρ, ρ_{sm},	=	density of water and material density of mud
ρ_{ss}	=	material density of sand
τ	=	shear stress
τ_b	=	boundary shear stress
τ^*	=	dimensionless Shields number for sand transport
τ^*_c	=	critical Shields number for sand transport
ξ	=	elevation of the water surface in the reservoir
ξ_m, ξ_{mp}	=	elevation of the interface of the muddy pond; nearly horizontal elevation of the muddy pond away from the barrier (in the case of overflow)
ξ_{ms}	=	elevation of the muddy pond at the barrier (sill)

References

Akiyama, J., and Stefan, H. (1984). "Plunging flow into a reservoir: Theory." *J. Hydraul. Eng.*, 110(4), 484-499.

Baddour, R. E. (1987). "Hydraulics of shallow and stratified mixing channel." *J. Hydraul. Eng.*, 113(5), 630-645.

Bell, H. S. (1942). "Stratified flow in reservoirs and its use in preventing silting." *Misc. Pub.* 491, U.S. Department of Agriculture, 46 p.

Brune, G. (1953). "Trap efficiency of reservoirs." *Trans.*, American Geophysical Union. 34 (3), 407-418.

Chikita, K. (1989). "A field study on turbidity currents initiated from spring runoffs." *Water Resour. Res.*, 25(2), 257-271.

De Cesare, G., Schleiss, A., and Hermann, F. (2001). "Impact of Turbidity Currents on Reservoir Sedimentation." *J. Hydraul. Eng.*, 127(1), 6-16.

Dietrich, E.W. (1982). "Settling velocities of natural particles." *Water Resour. Res.*, 18 (6), 1626 – 1682.

Engelund, F., and Hansen, E. (1972) *A monograph on sediment transport.* Technisk Forlag, Copenhagen, Denmark.

Fan, J., and Morris, G. (1992). "Reservoir sedimentation. I: Delta and density current deposits." *J. Hydraul. Eng.*, 118(3), 354-369.

Forel, F., (1885) "Les ravins sous-lacustres de fleuves glaciares. " *Comptes Rendus*, Academie de Sciences, Paris. T. 101, 725-728.

Garcia, M. H. (1993). "Hydraulic jumps in sediment-driven bottom currents." *J. Hydraul. Eng.*, 119(10), 1-24.

Graf, W. H. (1971). *Hydraulics of sediment transport*. McGraw-Hill.

Grover, N., and Howard, C. (1937). "The Passage of Turbid Water Through Lake Mead." *Trans.* ASCE 103, 720-790.

Kostic, S., and Parker, G. (2003a). "Progradational sand-mud deltas in lakes and reservoirs. Part 1: Theory and numerical model." *J. Hydraul. Res.*, 41(2), 127-140.

Kostic, S., and Parker, G. (2003b). "Progradational sand-mud deltas in lakes and reservoirs. Part 2. Experiment and numerical simulation." *J. Hydraul. Res.*, 41(2), 141-152.

Lambert, A. (1982). "Turbidity currents from the Rhine River on the bottom of Lake Constance." *Wasserwirtschaf*t, 72(4), 1-4 (in German).

Lane, E. (1954). "Some Hydraulic Engineering Aspects of Density Currents." Hyd. Lab. Report No Hyd-373, U.S. Bureau of Reclamation, Denver.

MacCormack, R. (1969). "The effect of viscosity in hypervelocity impact cratering." *Paper* 69-354, American Institute of Aeronautics and Astronautics, Cincinnati, Ohio.

Mahmood, K. (1987). "Reservoir sedimentation: Impact, extent and mitigation." *Technical paper* No.71, The World Bank, Washington D.C.

Morris, G., and Fan, J. (1997). *Reservoir sedimentation handbook.* Mc Graw Hill.

Normark, W. R., and Dickson, F. H. (1976). "Man-made turbidity currents in Lake Superior." *Sedimentology*, 23, 815-831.

Parker, G., Fukushima, Y., and Pantin, H. M. (1986). "Self-accelerating turbidity currents." *J. Fluid Mech.,* 171, 145-181.

Parker, G. and Toniolo, H. (submitted). "A note on the analysis of plunging density flows." *J. Hydraul. Eng.*, downloadable at: http://www.cee.uiuc.edu/people/parkerg/preprints.htm

Sloff, C.J. (1997). "Sedimentation in reservoirs." *Ph.D. Thesi*s, Technical University of Delft, the Netherlands, 269 p.

Smith W. O., Vetter, C.P., and Cummings, G. B. (1960). "Comprehensive survey of Lake Mead, 1948-1949." *Professional Paper* 295, U.S. Geological Survey, 254 p.

Stefan, H. and Hayakawa, N. (1972). "Mixing induced by an internal hydraulic jump." *Water Resour. Bull.*, 8(3), 531-545.

Swenson, J.B., Voller, V.R., Paola, C., Parker, G., and Marr, J. (2000). "Fluvio-Deltaic Sedimentation: A Generalized Stefan Problem." *Euro. J. Applied Math*., 11, 433–452.

Sloff, C.J. (1997). "Sedimentation in reservoirs." *Ph.D. Thesi*s, Technical University of Delft, the Netherlands, 269 p.

Smith W. O., Vetter, C.P. and Cummings, G. B. (1960). "Comprehensive survey of Lake Mead, 1948-1949." *Professional Paper* 295, U.S. Geological Survey, 254 p.

Stefan, H. and Hayakawa, N. (1972). "Mixing induced by an internal hydraulic jump." *Water Resour. Bull.*, 8(3), 531-545.

Swenson, J.B., Voller, V.R., Paola, C., Parker, G., and Marr, J. (2000). "Fluvio-Deltaic Sedimentation: A Generalized Stefan Problem." *Euro. J. Applied Math*., 11, 433–452.

Tannehill, J., Anderson, D., and Pletcher, R. (1997). *Computational Fluid Mechanics and Heat Transfer*, 2nd edition. Taylor & Francis,.

Toniolo, H., Lamb. M., and Parker, G. (in press(a)). "Depositional turbidity currents in diapiric minibasins on the continental slope: formulation and theory" *J. Sedimentary Res.*, downloadable at: http://www.cee.uiuc.edu/people/parkerg/preprints.htm

Toniolo, H., Parker, G., Voller, V., and Beaubouef, R. (in press(b)). "Depositional turbidity currents in diapiric minibasins on the continental slope: experiments, numerical simulation and upscaling." *J. Sedimentary Res.*, downloadable at: http://www.cee.uiuc.edu/people/parkerg/preprints.htm

Twichell, D. C., Cross, V. A., Hanson, A. D., Buck, B. J., Zybala, J. D., and Rudin, M. J. (2005). "Seismic architecture and lithofacies of turbidites in Lake Mead (Arizona and Nevada, U.S.A.), an analogue for topographically complex basins." *J. Sedimentary Res.*, 75(1), 134-148.

Wilkinson, D. L. and Wood, I. R. (1971). "A rapidly varied flow phenomenon in a two-layer flow." *J. Fluid Mech.* 47(2), 241-256.

de Vries, M. (1965). "Consideration about non-steady bed-load-transport in open channels." *Proc.* IAHR, 11th Congress, Vol. 3, Paper 3.8, 11p.

FIGURE CAPTIONS

Figure 1. Sketch of the geometric configuration considered in the formulation. The flow is from left to right. The interface of the muddy pond is drawn below the lip of the dam, but it may be above the lip as well.

Figure 2. Pattern of sediment deposition from the Colorado River as it enters Lake Mead. From Graf (1971), based on an original in Smith et al. (1960).

Figure 3. Sketch of the flow of a turbidity current into a submerged basin in the deep sea. The incoming turbidity current is supercritical. The downstream barrier of the basin forces an internal hydraulic jump to subcritical flow, forming a muddy pond. The elevation of the interface of the muddy pond may be below or above the downstream lip of the basin.

Figure 4. Sketch showing the formation of a settling interface and water detrainment in a cylinder containing a dilute suspension of mud of uniform size.

Figure 5 a) Reservoir with a muddy pond, and with water overflowing from a vent. The interface of the muddy pond is drawn below the vent, but may be above the vent as well, b) Modification of the configuration of Fig. 5a so that ambient water is ponded on both sides of the downstream barrier. Two interfaces for the muddy pond are shown, one below the barrier and one above it.

Figure 6. Experimental configuration.

Figure 7. Grain size distributions of black sand and white mud (glass beads) used in the experiment.

Figure 8. Bed elevations at different times during the experiment, as well as the elevation of the free surface of the clear water. The flow was from left to right.

Figure 9. Photographs illustrating the final deposit. The deposit thickness is very uniform downstream of the fluvial delta; it is composed almost exclusively of white silt. Sediment is seen to be deposited both within and beyond the downstream barrier of the basin. Nearly all the black sand and a small portion of the white silt was deposited in the fluvial topset and foreset. The flow was from right to left.

Figure 10. Diagram illustrating the vertical profiles of suspended sediment concentration at various times for the experiment.

Figure 11. Photograph of the horizontal settling interface and the water surface in the ponded zone of reservoir during the experiment.

Figure 12. Photograph showing the downstream end of the reservoir during the experiment. The interface between muddy and clear water is located above the downstream overflow lip. The flow direction was from right to left.

Figure 13. Vertical profiles of the geometric mean size of the suspended sediment at different times during the experiment.

Figure 14. Long profile of the grain size associated with the peak of the probability density of grain size for the samples of bed material collected at the end of experiment. Flow was from left to right.

Figure 15. Plot of profiles of bed elevation at various times, along with plots of the final water surface elevation and final profile of the interface of the

turbidity current obtained from the numerical simulation of the experiment. Flow is from left to right.

Figure 16. The plot shows the elevation of the foreset-bottomset break as a function of the streamwise position of the same break predicted by the numerical simulation. Delta progradation was thus accompanied by bottomset aggradation.

Figure 17. Plot of measured and simulated profiles for deposit thickness at the end of the experiment (t = 60 min). Flow was from left to right.

Figure 18. Result of a field-scale simulation showing the bed profile at four times, the water surface profile at the end of the simulation and the profile of the interface of the turbidity current at the end of the simulation. Flow was from left to right.

Figure 19. Plot showing the interface of the muddy pond as a function of time, as predicted by the field-scale simulation. Initially the muddy pond does not overflow the barrier (sill), but at later times it does.

Figure 20. Plot of trap efficiency of sediment as a function of time predicted by the field-scale simulation.

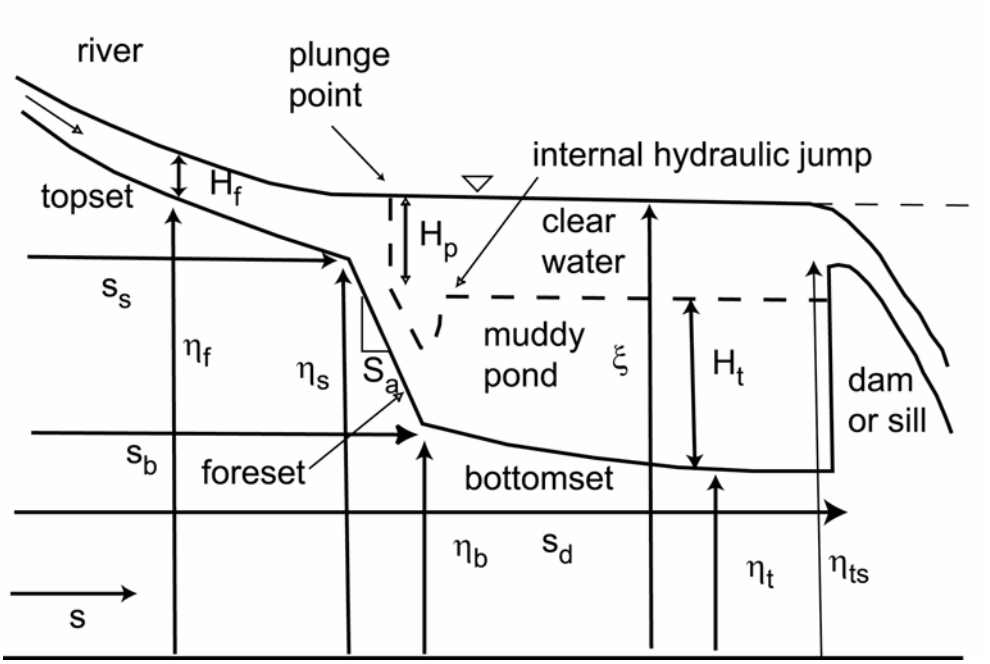

Figure 1.

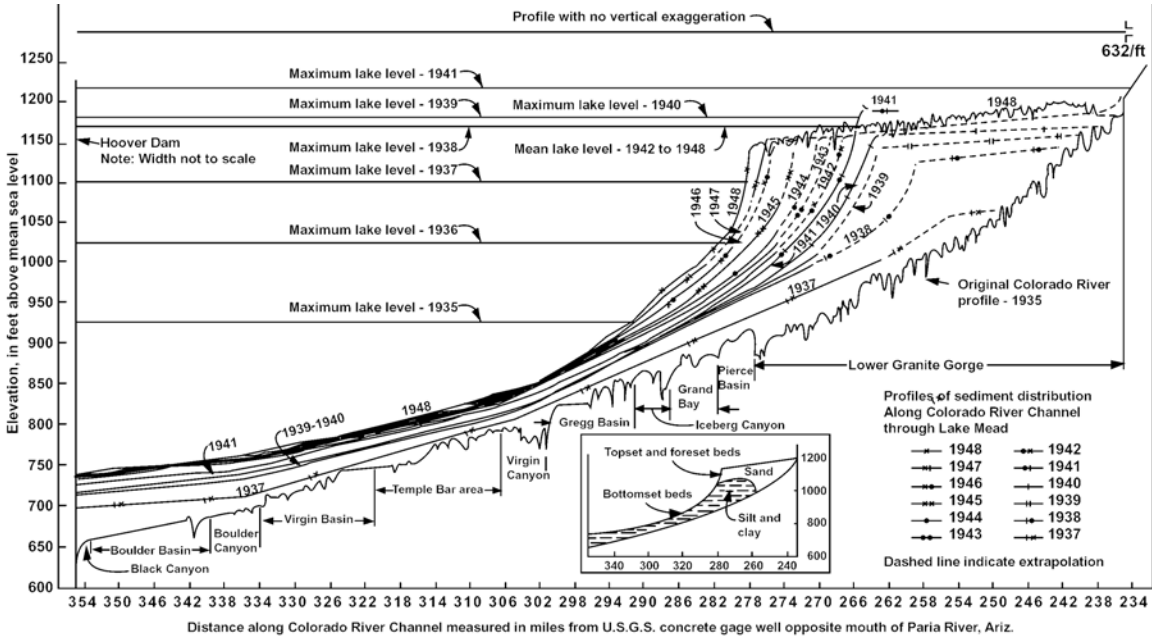

Figure 2.

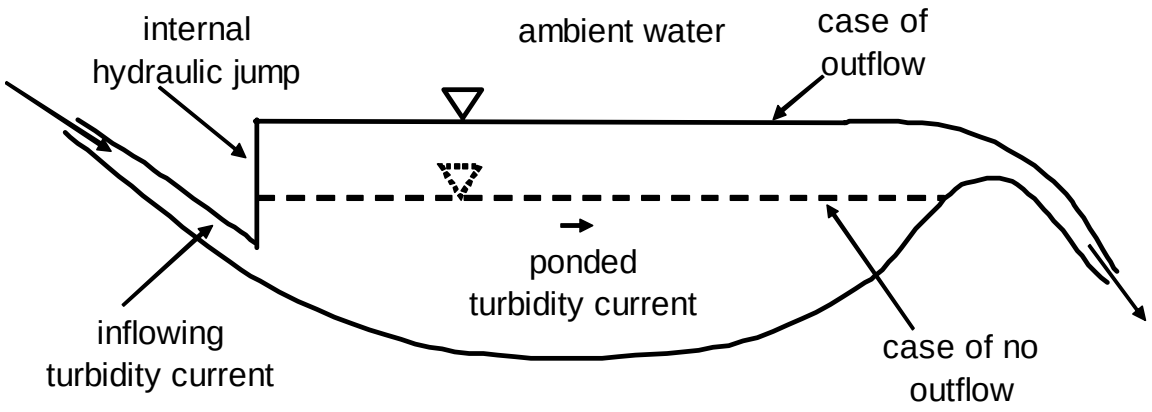

Figure 3.

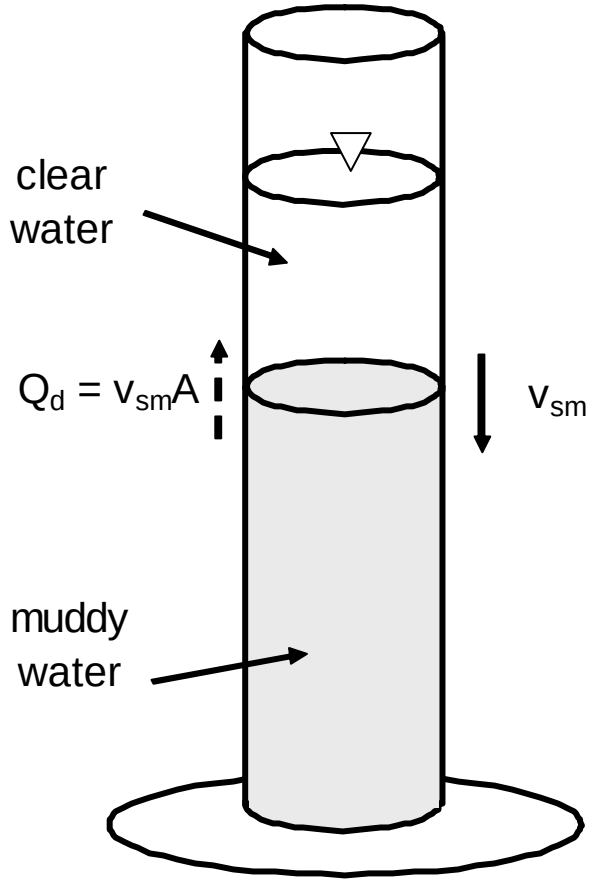

Figure 4.

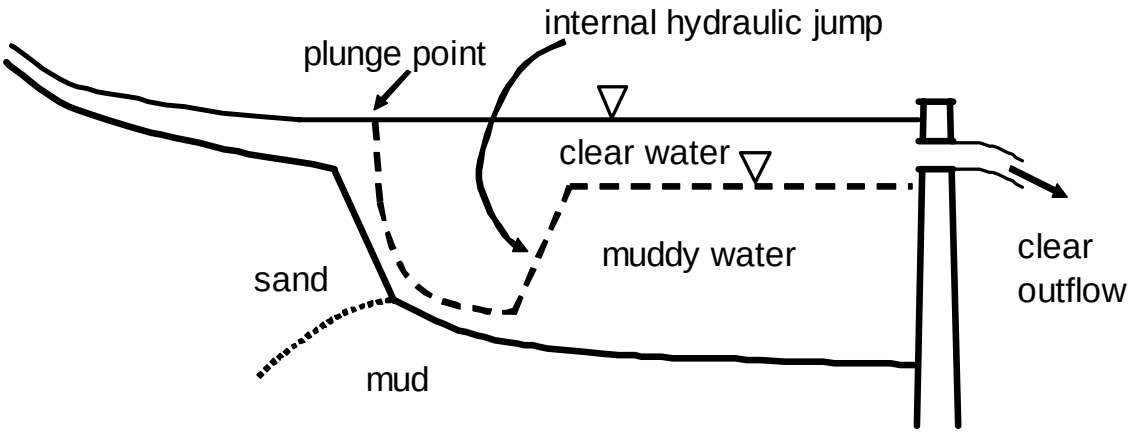

Figure 5a.

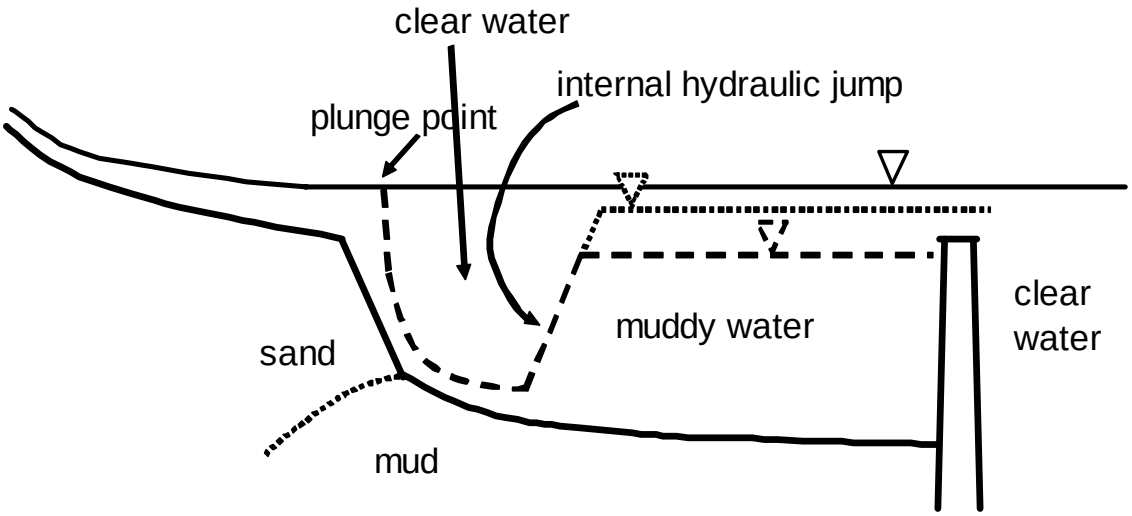

Figure 5b.

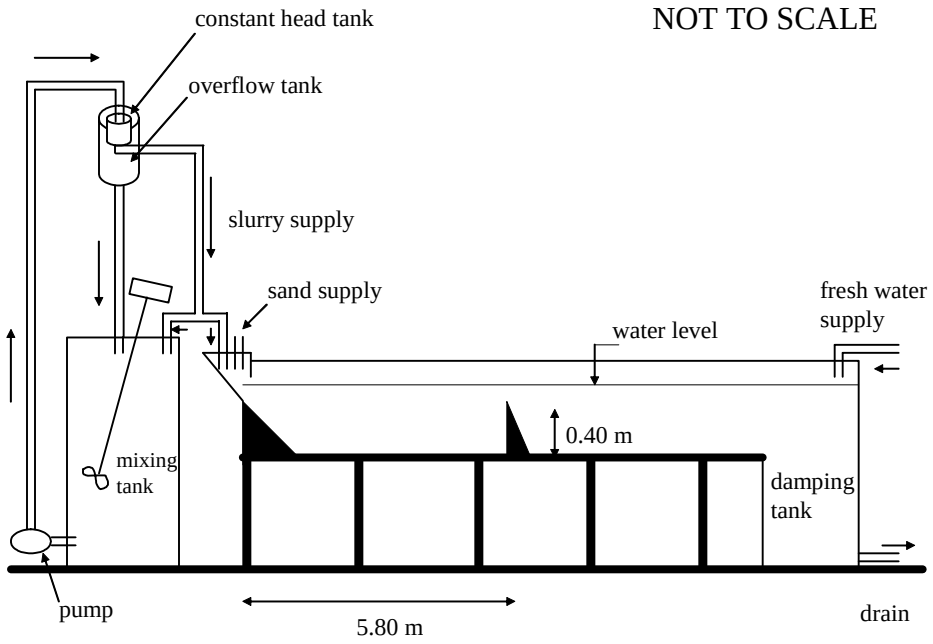

Figure 6.

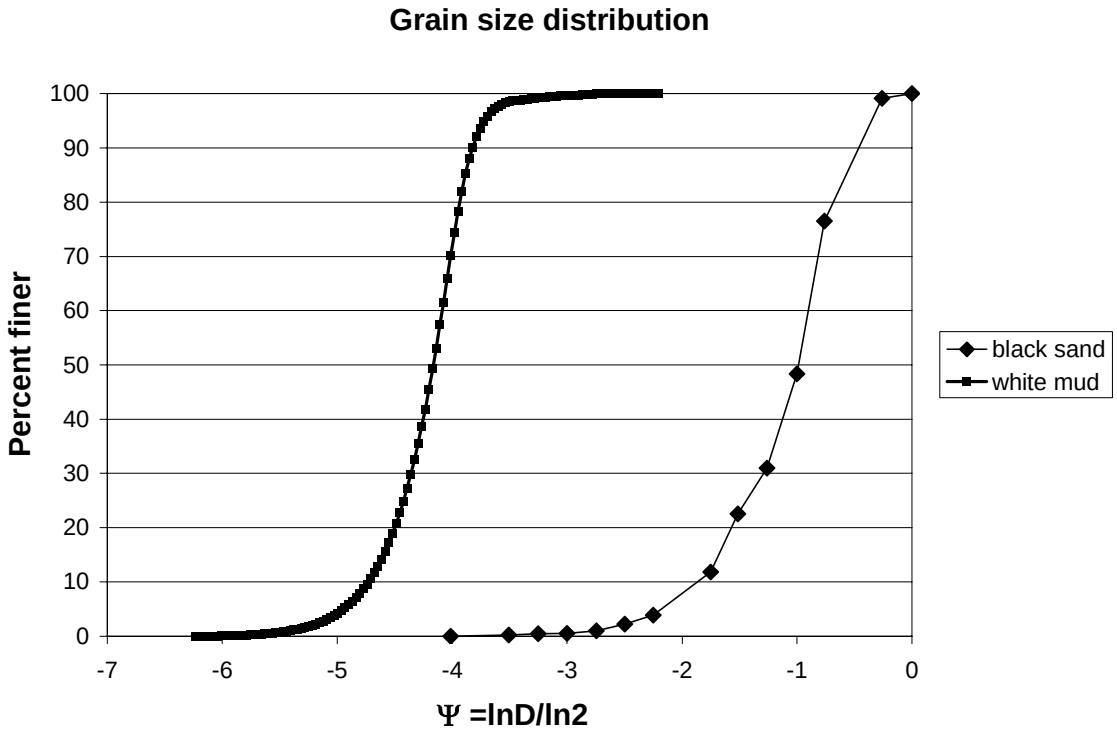

Figure 7.

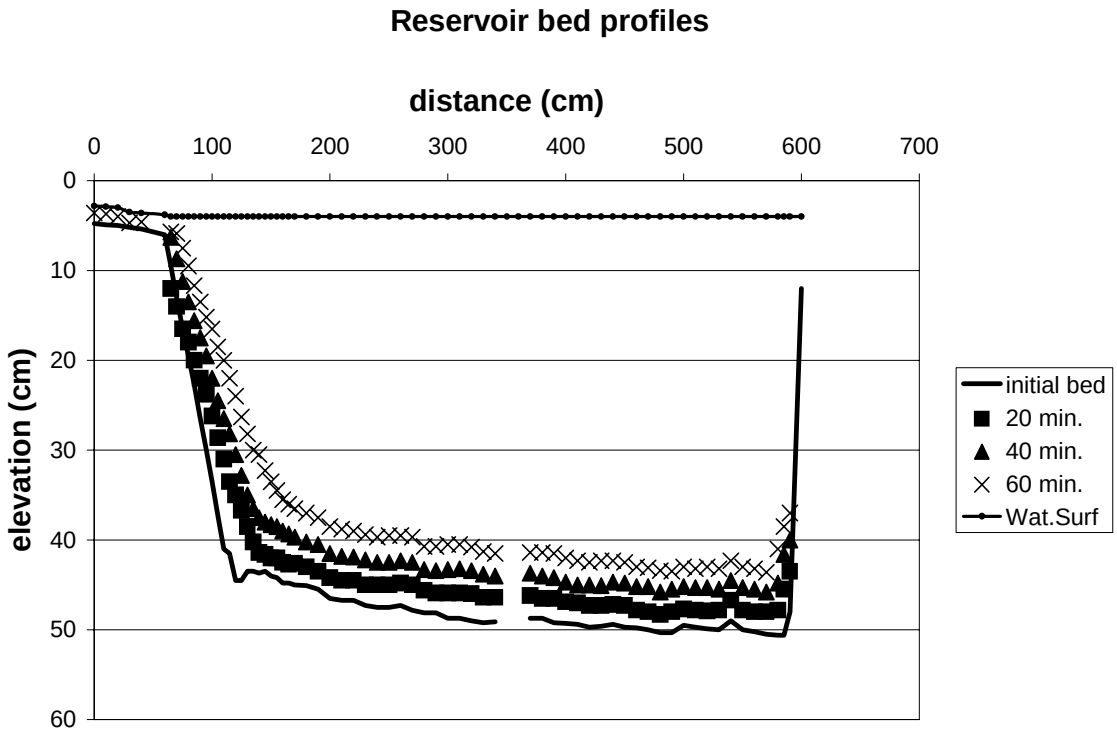

Figure 8.

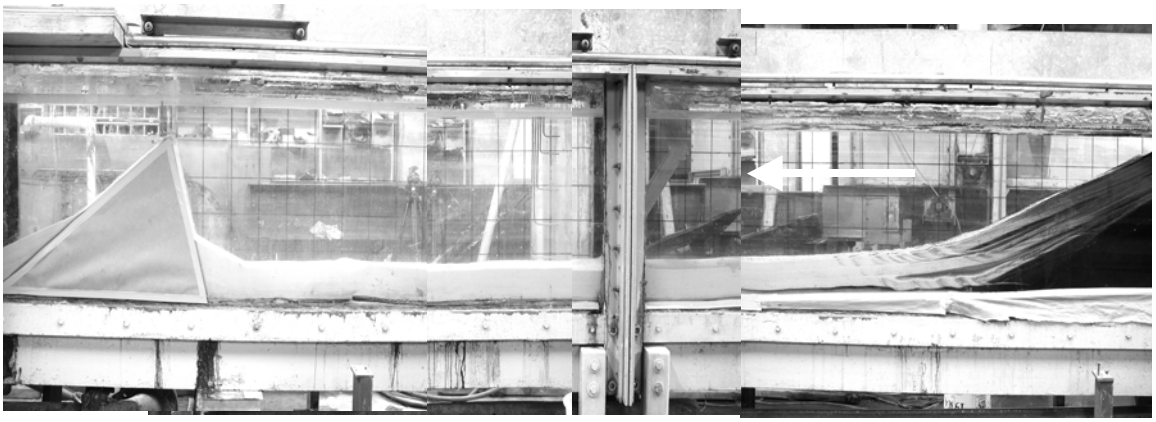

Figure 9.

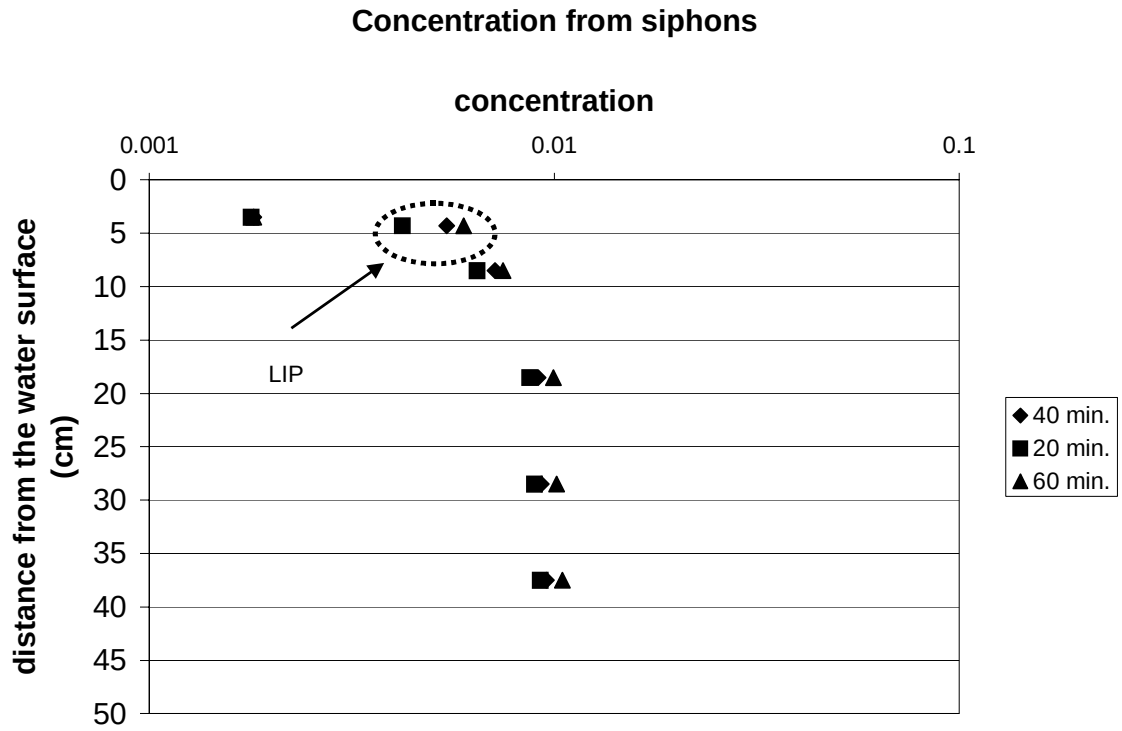

Figure10.

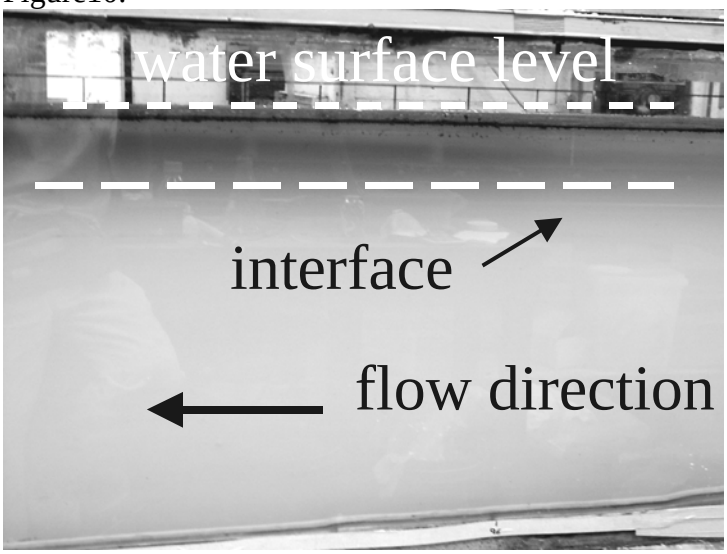

Figure 11.

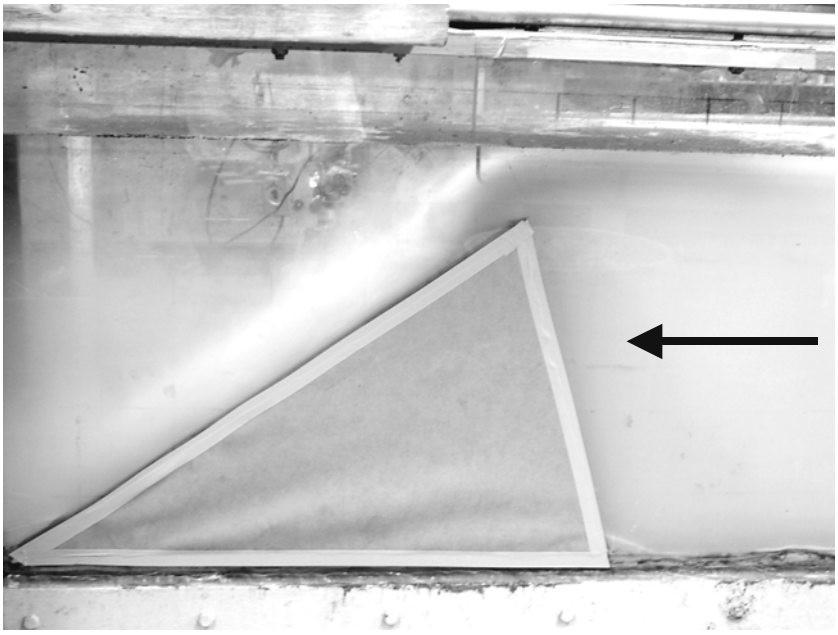

Figure12.

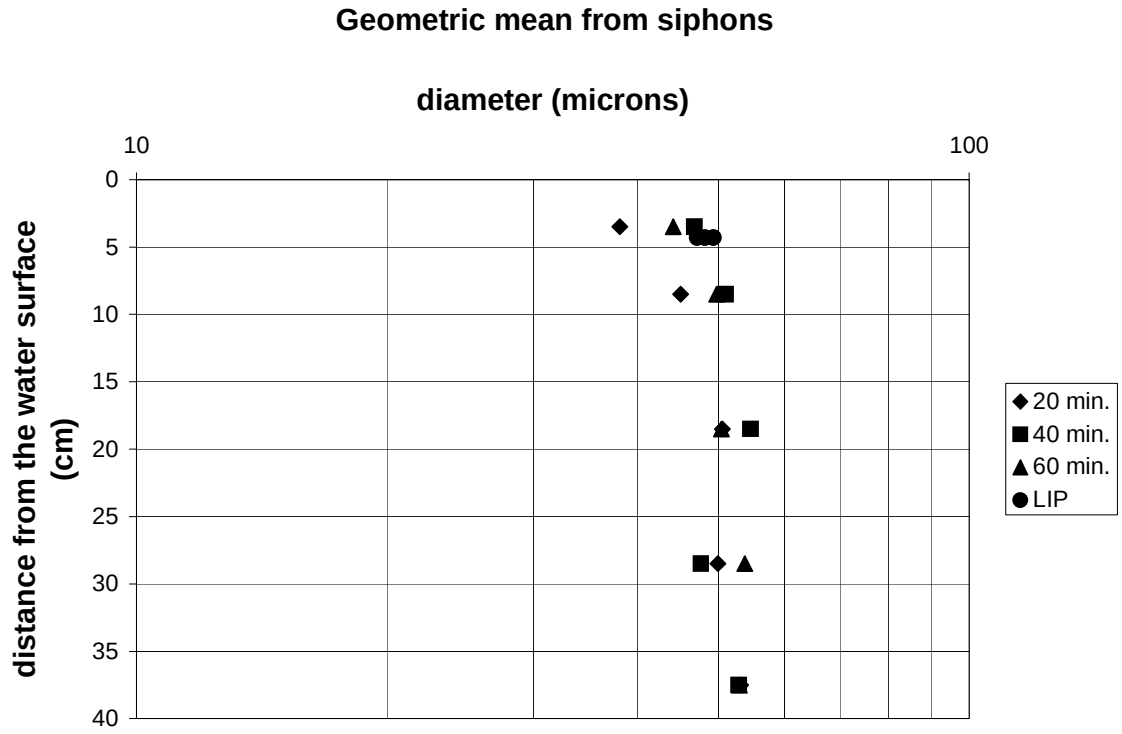

Figure 13.

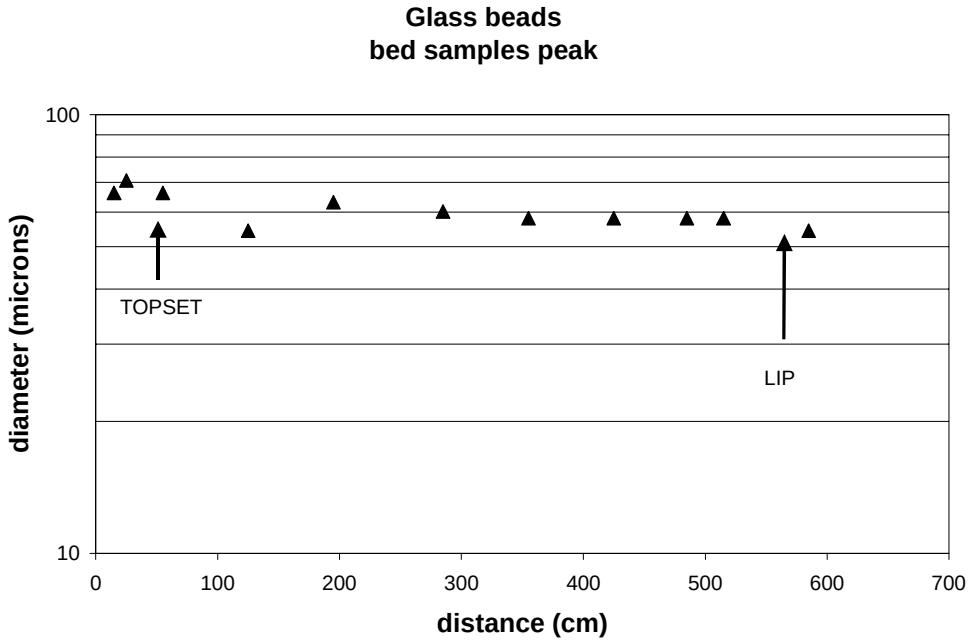

Figure 14.

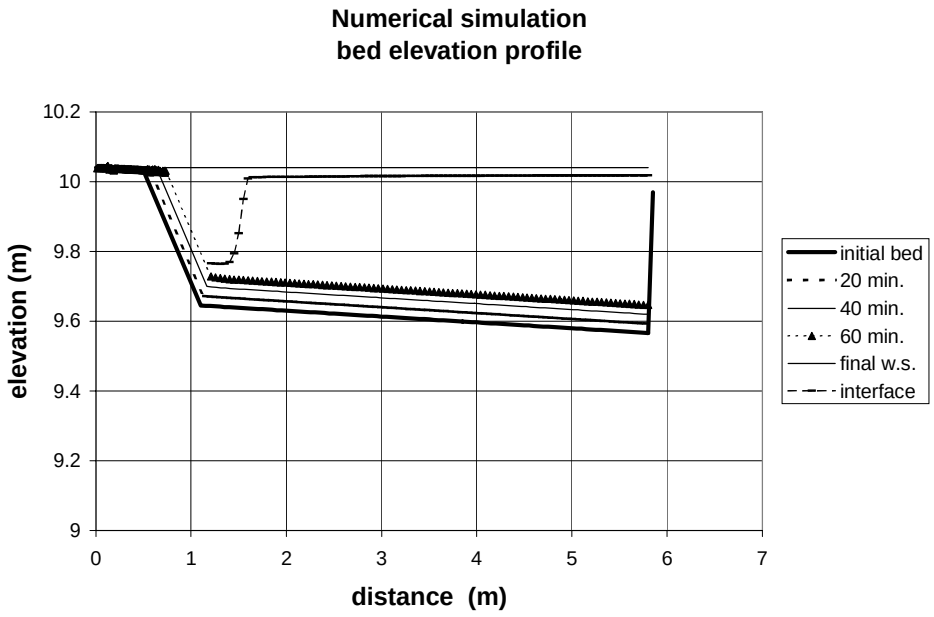

Figure 15.

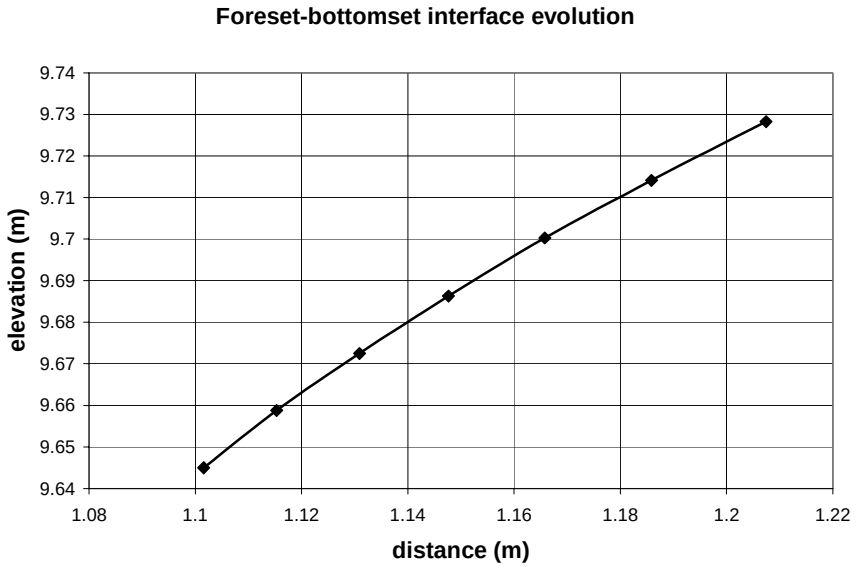

Figure 16.

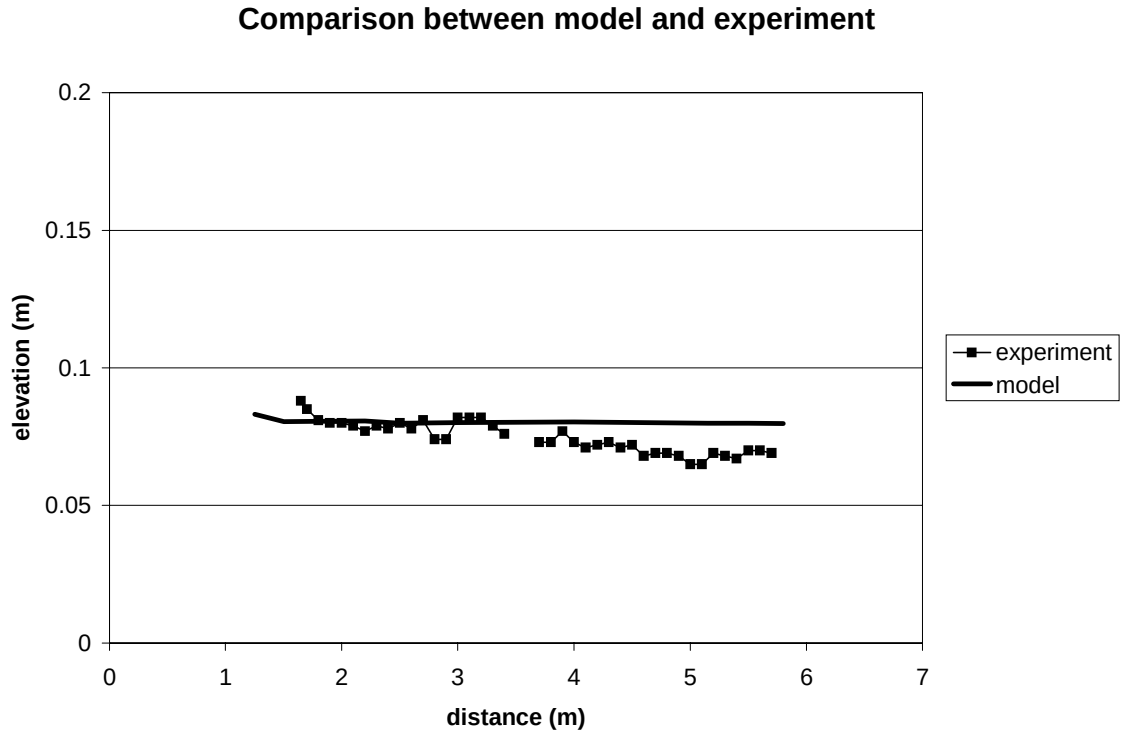

Figure 17.

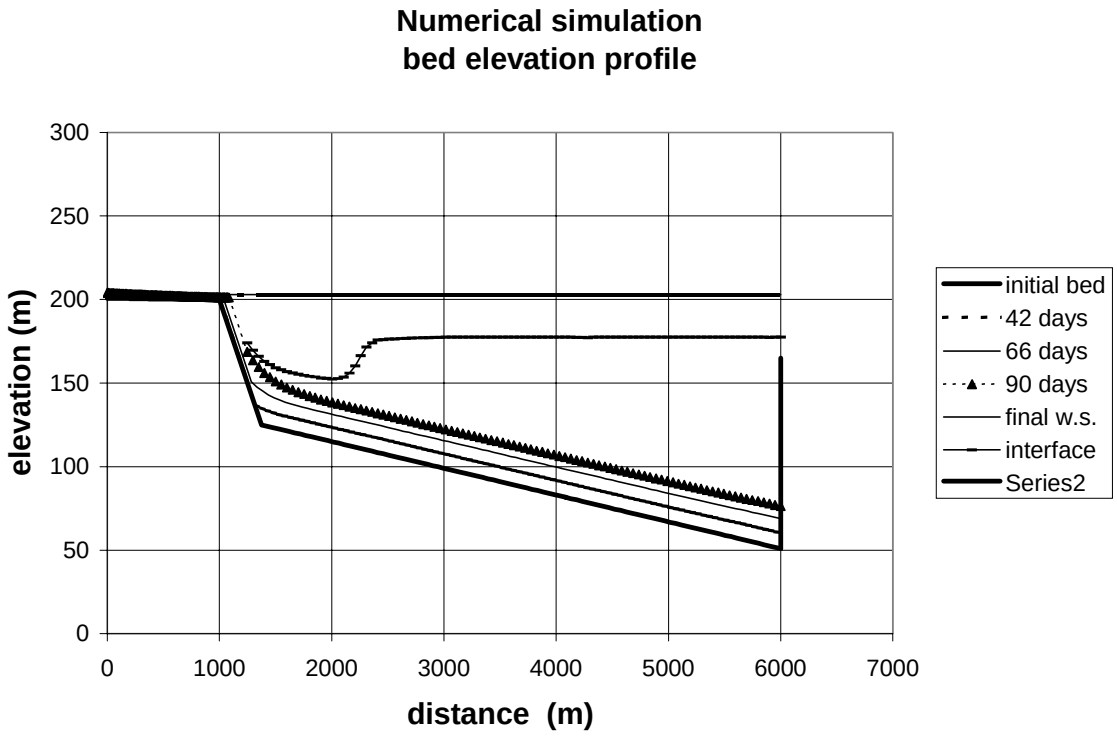

Figure 18.

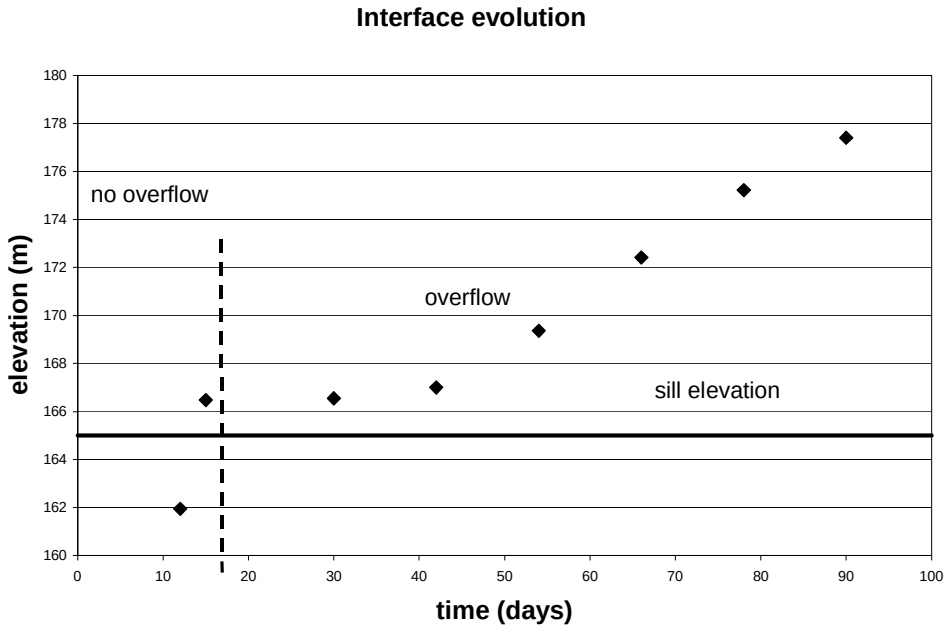

Figure 19.

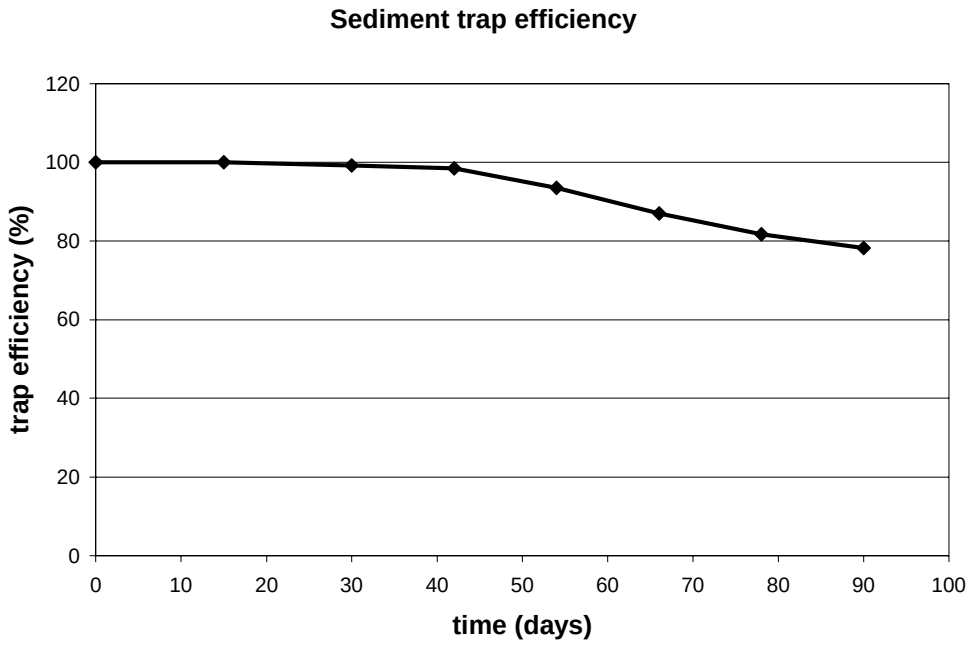
Sediment trap efficiency
trap efficiency (%)
120
100
80
60
40
20
0
0
10
20
30
40
50
60
70
80
90
100
time (days)

Figure 20.